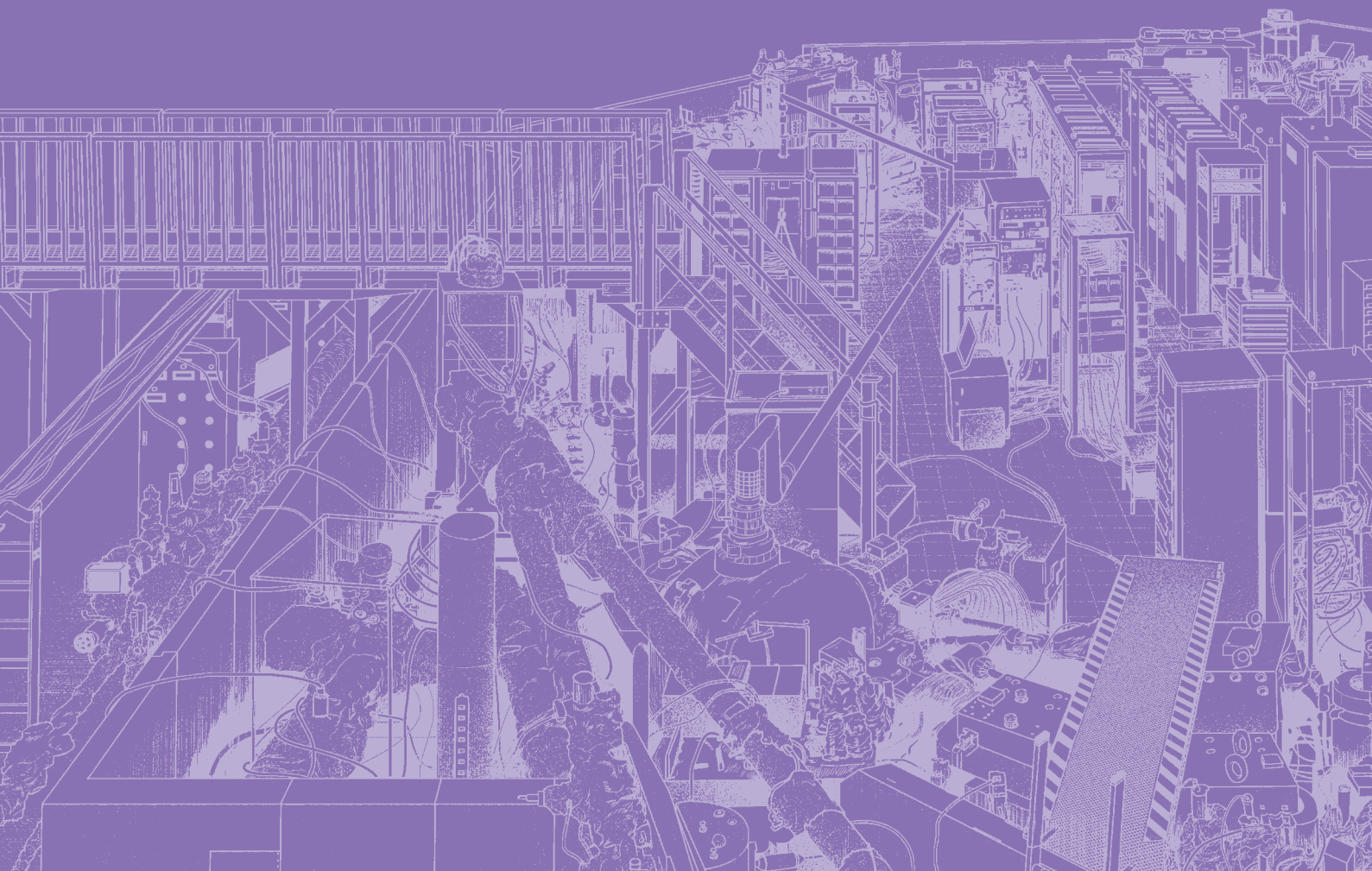


III-4

Surface,
Interface and
Thin Films





BL6U

Fermiology of a Kagome Superconductor $\text{Cs}(\text{V}_{1-x}\text{Nb}_x)_3\text{Sb}_5$ Revealed by Momentum Microscope

T. Kato¹, K. Nakayama¹, Y. Li^{2,3,4}, Z. Wang^{2,3,4}, S. Souma^{5,6}, F. Matsui⁷,
T. Takahashi¹, Y. Yao^{2,3} and T. Sato^{1,5,6,8}

¹Department of Physics, Graduate School of Science, Tohoku University, Sendai 980-8578, Japan

²Centre for Quantum Physics, Key Laboratory of Advanced Optoelectronic Quantum Architecture and Measurement (MOE), School of Physics, Beijing Institute of Technology, Beijing 100081, P. R. China

³Beijing Key Lab of Nanophotonics and Ultrafine Optoelectronic Systems, Beijing Institute of Technology, Beijing 100081, P. R. China

⁴Material Science Center, Yangtze Delta Region Academy of Beijing Institute of Technology, Jiaxing, 314011, P. R. China

⁵Advanced Institute for Materials Research (WPI-AIMR), Tohoku University, Sendai 980-8577, Japan

⁶Center for Science and Innovation in Spintronics (CSIS), Tohoku University, Sendai 980-8577, Japan

⁷UVSOR Synchrotron Facility, Institute for Molecular Science, Okazaki 444-8585, Japan

⁸International Center for Synchrotron Radiation Innovation Smart (SRIS), Tohoku University, Sendai 980-8577, Japan

Recently, AV_3Sb_5 compounds (where A represents an alkali metal K, Rb, or Cs) have been discovered to host an ideal two-dimensional kagome lattice formed by V atoms [Fig. 1(a)]. These materials undergo a charge density wave (CDW) transition below the critical temperature (T_{CDW}) of 78-103 K. The CDW transition is characterized by lattice distortions with the star-of-David or inverse star-of-David patterns. Notably, the CDW phase exhibits intriguing properties, including the coexistence with superconductivity, time-reversal symmetry breaking, and nematicity. Understanding the origin of the CDW in AV_3Sb_5 and its interplay with other properties is currently a hot topic in condensed matter physics. One useful approach to study this issue is to perturb the CDW phase by varying key physical parameters such as pressure and carrier concentrations. In this regard, chemical substitution in the crystal, which can adjust chemical pressure and/or carrier concentrations, is a promising strategy.

In this study, we performed an angle-resolved photoemission spectroscopy (ARPES) study on Nb-substituted CsV_3Sb_5 , $\text{Cs}(\text{V}_{1-x}\text{Nb}_x)_3\text{Sb}_5$, with $x = 0, 0.03$, and 0.07 [1]. The substitution of V with isovalent Nb results in a reduction of T_{CDW} , while simultaneously enhancing the superconducting transition temperature (T_c) [Fig. 1(b)].

High-quality single crystals of $\text{Cs}(\text{V}_{1-x}\text{Nb}_x)_3\text{Sb}_5$ were synthesized by the self-flux method. ARPES measurements were carried out by using momentum microscope KREIOS 150 MM (SPECS) at BL6U [2].

In Fig. 1(c), we present the experimentally determined Fermi surface in the normal state at $T = 120$ K (above T_{CDW}) for the highest Nb concentration ($x = 0.07$). The use of a momentum microscope allowed to collect photoelectrons over a wide momentum space, enabling a comprehensive observation of multiple Fermi surfaces. Specifically, we observed a circular pocket centered at Γ , which is derived from the p orbital of Sb atoms embedded in the kagome lattice plane, and a

large hexagonal pocket at Γ and triangular pockets at K, both of which originate from the $3d$ orbitals of the V kagome lattice. A comparison of the Fermi surface at $x = 0.07$ with that at $x = 0$ reveals intriguing trends: the circular pocket expands with increasing x , while the triangular pocket shrinks. The significant impact of the observed band shift is a lifting of the saddle point near the M point away from the Fermi level. Since T_{CDW} becomes higher when the saddle point is located at closer to the Fermi level, a large density of states of the saddle point plays a key role in stabilizing CDW. Additionally, our findings suggest that the enhancement of T_c through Nb substitution is partly attributed to the expansion of the circular pocket.

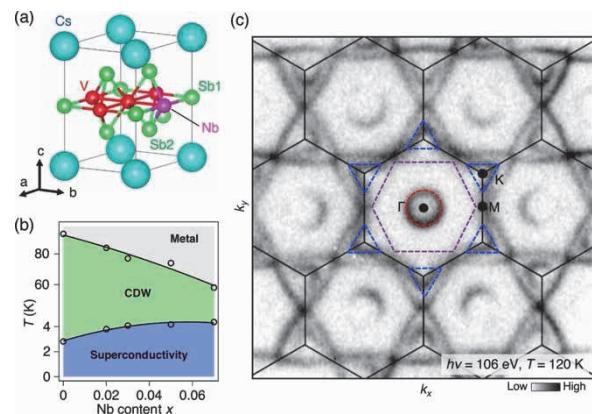


Fig. 1. (a) Crystal structure and (b) phase diagram of $\text{Cs}(\text{V}_{1-x}\text{Nb}_x)_3\text{Sb}_5$. (c) ARPES intensity at the Fermi level plotted as a function of two-dimensional wave vector. Red, purple, and blue dashed lines are guides for the eyes to trace the experimental Fermi surfaces.

[1] T. Kato *et al.*, Phys. Rev. Lett. **129** (2022) 206402.

[2] F. Matsui *et al.*, Jpn. J. Appl. Phys. **59** (2020) 067001.

Mg K-edge NEXAFS of MgO, Mg(OH)₂ and MgCO₃

E. Kobayashi¹, S. Yoshioka² and K. K. Okudaira³

¹Kyushu Synchrotron Light Research Center, 8-7 Yayoi-gaoka, Tosu, Saga 841-0005, Japan

²Graduate School of Engineering, Kyushu University, 744 Motoooka Nishi-ku Fukuoka 819-0395 Japan

³Graduate School of Science and Engineering, Chiba University,
1-33 Yayoi-cho Inage-ku, Chiba 263-8522, Japan

In recent years, organic photovoltaic (OPV) has been attracting attention as a low-cost, lightweight battery that replaces conventional solar cells. Metal oxides play an essential role as an electron and a hole transport layer (ETL and HTL) material. [1,2] In order to further improve the characteristics of these charge transport layers, it is necessary to understand the band structure. Near-edge x-ray absorption fine structure (NEXAFS) spectroscopy is a powerful tool for investigating the unoccupied state of band structure of materials. When discussing the band structure, information on the position of the unoccupied bottom is important. It is necessary to know the effects on the bottom of the unoccupied band when metal oxides are contaminated by atmospheric component such as OH and CO₂. Therefore, we measured the unoccupied state of MgO, Mg(OH)₂ and MgCO₃ · xH₂O generated by the adsorption of OH and CO₂ on the MgO surface.

NEXAFS spectra of the MgO, Mg(OH)₂ and MgCO₃ · xH₂O powders using both total electron yield (TEY) and partial fluorescence yield (PFY) modes were measured at the beamline 2A of the UVSOR in the Institute of Molecular Science. For TEY, the drain current from the sample was measured. For PFY, fluorescence X-rays were collected using an energy dispersible silicon drift detector (SDD). All experiments were performed at room temperature.

Figure 1 shows the Mg K-edge NEXAFS spectra of MgO, Mg(OH)₂ and MgCO₃ · xH₂O powder obtained from TEY mode. The peak positions of MgO, Mg(OH)₂ and MgCO₃ · xH₂O spectra are different. This suggests that their structures are different. On the other hand, the rising positions of the spectra of MgO, Mg(OH)₂ and MgCO₃ · xH₂O are very similar. This suggests that the bottom of the unoccupied band is the same. Figure 2 shows the Mg K-edge NEXAFS spectra of MgO, Mg(OH)₂ and MgCO₃ · xH₂O powder obtained from PFY mode. The rising positions of the spectra of MgO, Mg(OH)₂ and MgCO₃ · xH₂O are very similar. It was

found that the bottom of the unoccupied state of MgO was not affected by contamination by atmospheric component such as OH and CO₂.

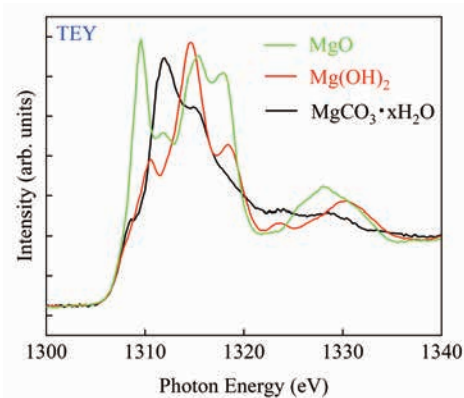


Fig. 1. Mg K-edge NEXAFS spectra of MgO, Mg(OH)₂ and MgCO₃ · xH₂O powder obtained from TEY mode.

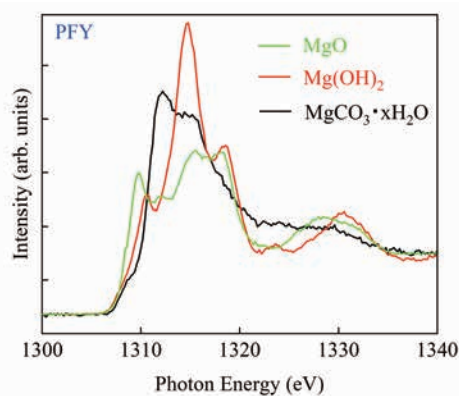


Fig. 2. Mg K-edge NEXAFS spectra of MgO, Mg(OH)₂ and MgCO₃ · xH₂O powder obtained from PFY mode.

- [1] I. Ierides *et al.*, *J. Mater. Chem. C* **9** (2021) 3901.
[2] Y. -J. Lee *et al.*, *Adv. Energy Mater.* **2** (2012) 1193.

BL2A

Structural Analyses of Silicon Atoms in a Zero-dimensional Metal-atom Encapsulating Silicon Cage Clusters by X-ray Absorption Spectroscopy

A. Nakajima and T. Inoue

Department of Chemistry, Faculty of Science and Technology, Keio University, 3-14-1 Hiyoshi, Kohoku-ku, Yokohama 223-8522, Japan

Since silicon (Si) element belongs to the same group as carbon, it has been highly expected to create novel low-dimensional compounds as fullerene and carbon nanotube. In zero-dimensional silicon nanoclusters, it has been found that metal-atom encapsulating silicon cage, $M@Si_{16}$ superatom (SA), can be generated in a gas-phase synthesis [1, 2]. In this study, the X-ray absorption fine structure analysis (XAFS), especially the extensive X-ray absorption fine structure analysis (EXAFS), has been applied to thin films of $M@Si_{16}$ SA deposited on a solid surface to reveal the structural information, compared with the structure obtained by quantum chemical calculations.

The $Ta@Si_{16}$ SA, composed of tantalum (Ta) and Si, was generated using a pulsed magnetron sputtering system, and $Ta@Si_{16}$ SA cations were deposited on a highly oriented pyrolytic graphite (HOPG) substrate that was set on a wobble stick, as ten layers with a spot of 6-8 mm in diameter. The deposited substrate was kept in vacuum with an ion pump and transported from Keio University to UVSOR, where an ion pump was used with a nickel hydride battery (pumping speed 20L/s). The battery (24 V, 2000 mA h) can work in 10 hours, which covers the transportation time, and XAFS measurements of the Si K-edge were performed at the BL2A beamline (Fig. 1). Absorption of Si atoms was measured by the fluorescence method. The structure was identified by comparing the obtained EXAFS spectrum with the theoretically calculated FEFF spectrum of three structural isomers (T_d , D_{4d} , and C_{3v}).

For the deposited $Ta@Si_{16}$ SA samples, XANES and EXAFS measurements were performed for the Si K-edge at 1800 to 2400 eV in the soft X-ray region (Fig. 2). For monitoring the incident light intensity, the scattered intensity of the copper mesh was used instead of gold mesh, because there is no XAFS of copper in the measurement energy region. However, the optics in the beamline inevitably contain gold-coated ones, and then X-ray absorption based on gold appears above 2000 eV; the light intensity decreases, where Si K-edge signals should be observed from the thin $Ta@Si_{16}$ SA films. Although proper normalization of the incident light intensity had been tried with the scattered fluorescence from the measurement sample itself, the incident light intensity could not be accurately evaluated, and then the measurement energy range was squeezed to 1800-2000 eV ($k = 3 - 7 \text{ \AA}^{-1}$). The EXAFS vibrations in the soft X-ray region were compared

between the obtained spectra and the theoretically calculated FEFF spectra of structural isomers to obtain the structural information.



Fig. 1. Photo of the connected chamber transported from Keio University.

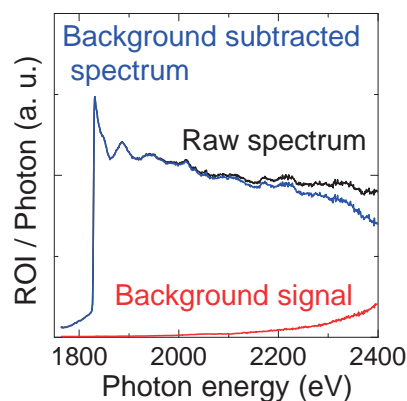


Fig. 2. Si K-edge XAFS Spectra for the deposited $Ta@Si_{16}$ SA samples. The spectrum in blue was obtained by subtracting background signal in red from raw spectrum in black. The spectrum in 1800-2000 eV was used for the structural analyses.

[1] H. Tsunoyama, H. Akatsuka, M. Shibuta, T. Iwasa, Y. Mizuhata, N. Tokitoh and A. Nakajima, *J. Phys. Chem. C* **121** (2017) 20507.

[2] H. Tsunoyama, M. Shibuta, M. Nakaya, T. Eguchi and A. Nakajima, *Acc. Chem. Res.*, **51** (2018) 1735.

Annealing Effects on Surface Electronic Structure of MoO₃ Nanoparticles by UPS

K. K. Okudaira¹ and S. Ishii²,

¹Graduate School of Engineering, Chiba University, 1-33 Yohoi-cho, Inage-ku Chiba 263-8522, Japan

²Graduate School of Science and Engineering, Chiba University,
1-33 Yohoi-cho, Inage-ku Chiba 263-8522, Japan

Organic photovoltaic (PV) cells have been the hot research topic in recent years due to their advantages of low-cost manufacturing, light weight and good flexibility. Among these PV cells, solution-processed bulk heterojunction PV cells with donor–acceptor (D–A) blends sandwiched between the anode and cathode are the most promising alternative to realize large-scale production. In bulk heterojunction PV cells, the charges generated in the active layer upon light absorption are transported via D–A networks and collected by the electrodes to realize light-electricity conversion. Recently, the transition metal oxides (TMOs) were inserted between the electrodes and organic active layer to prevent the leakage of undesired charged carrier to electrode as well as to promote the charged carrier transfer. [1] The efficiency of these electron transfer layer (ETL) and hole transfer layer (HTL) largely depend on the surface electronic structure of the TMO layer.

In this work we prepared MoO₃ nanoparticles (NPs) films with different annealing atmosphere and estimated the electronic structure of MoO₃ NPs by ultraviolet photoelectron spectroscopy (UPS) measurements to estimate the effect of annealing on the surface electronic structure and the work function.

UPS measurements were performed at the beam line BL2B of the UVSOR storage ring at the Institute for Molecular Science at the photon energy ($h\nu$) of 28 eV. MoO₃ NPs were synthesized via solvothermal method. [2] The thin films of MoO₃ NPs were deposited on ITO by spin casting (denoted as “non”). The films were annealed at 500°C in air and hydrogen atmosphere (denoted as “in air” and “in H₂”, respectively). The mean size of synthesized MoO₃ NPs was about 10 ~ 30 nm using TEM measurements.

The whole spectral structure of MoO₃ thin films by annealing in H₂ atmosphere is almost same as that of non annealing as shown in Fig. 1 (a). On the contrary, by annealing in air, the position of valence band top (VBT) is shifted to higher binding energy by about 0.3 ~ 0.4 eV. It is expected that the Fermi level leaves from VBT due to the formation of defect states just

above the Fermi level by annealing in air. Furthermore, the work function of MoO₃ films by annealing in air is larger than that of non annealing MoO₃ films by about 0.2 eV. This vacuum level shift is considered by the interfacial dipole formation due to the introducing the hydroxyl group to the surface of the MoO₃ film by annealing in air.

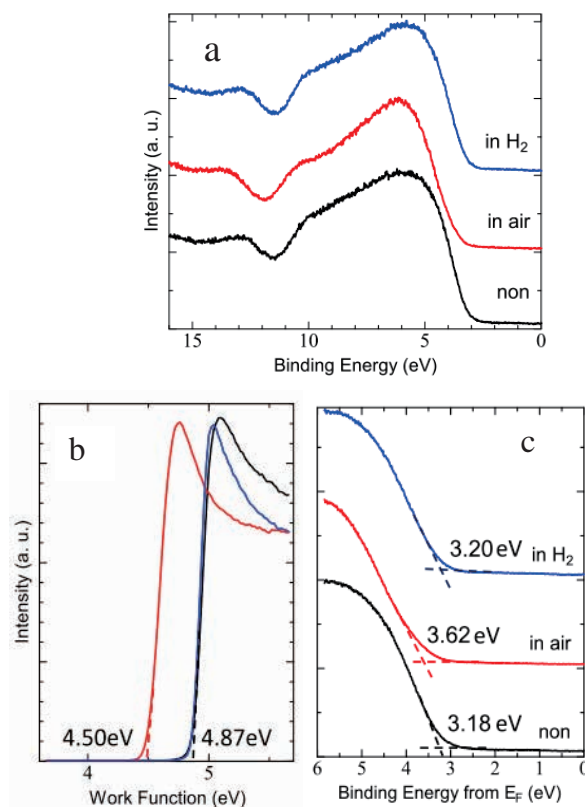


Fig. 1. UPS of MoO₃ NPs at $h\nu = 28\text{eV}$ (a) in the valence band region (b) in the secondary cut-off and (c) in the valence top region.

[1] F. Liu *et al.*, Sol. Energy Mater. Sol. Cells **94** (2010) 842.

[2] W.-S. Kim *et al.*, J. Nanopart. Res. **12** (2010) 1889.

BL3U

X-ray Absorption Spectroscopy Study of 4-MBA and Cysteine on Gold Surfaces

F. Sato¹, I. Sakaida¹, S. Ohno¹ and M. Nagasaka²

¹Graduate School of Engineering Science, Yokohama National University, Yokohama 240-8501, Japan

²Institute for Molecular Science, Okazaki 444-8585, Japan

It is important to understand the behavior of biomolecules on solid surfaces for the application to medical device, biosensor and biocompatible material. It is essential to study the adsorption and desorption behavior of biomolecules and their response to the applied electric fields. It is of particular importance to analyze the dynamic behavior of biomolecules on a surface in electrolyte solutions, which is close to the realistic condition in the body of living creatures [1,2].

In the present study, potential-dependent adsorption/desorption behavior of 4-mercaptobenzoic acid (4-MBA) and cysteine on Au membrane surfaces have been investigated using soft X-ray absorption spectroscopy (XAS) in the transmission mode. The experiments were performed on the soft X-ray undulator beam line at UVSOR-III, BL3U. We used H₂SO₄ and KOH as the electrolyte solution. For the adsorption of 4-MBA molecules, the samples were immersed in 1mM 4-MBA/ethanol solution for more than 30 min. For the adsorption of cysteine molecules, the samples were immersed in 1mM cysteine/K-OH solution for more than 1 hour.

In our previous study, we have studied the adsorption/desorption behavior of 4-MBA on Au films using surface differential reflectance spectroscopy (SDRS) combined with cyclic voltammetry (CV) [3]. The key issue was the interaction between functional group (-COOH) and Au films through Coulomb interaction depending on the applied biases and pH conditions. Redox processes involving charge transfer were clearly observed with CV and the relation between the change in the reflectance spectra and the peaks in CV was investigated in detail. Interestingly, we found some precursor phenomena to cause significant changes in the reflectance spectra with no corresponding signal in CV. This indicates that such changes in the reflectance spectra are not due to the charge-transfer-type reactions but rather to the subtle change in the orientation/conformation of 4-MBA molecules. We also observed similar effects for cysteine.

To our knowledge, there has been no serious effort to study the 4-MBA/Au and cysteine/Au systems using XAS in terms of the aforementioned precursor phenomena. At the initial stage, we have tried to observe the effects on Au(111). However, we could not obtain the clear data showing the adsorption/desorption behavior of 4-MBA, though they are

confirmed with CV measurements.

Here, we used an Au membrane as the substrate which has polycrystalline structure. Our CV data reveal that there should be Au(111) part on the surface, and that clear feature for adsorption/desorption for both 4-MBA and cysteine are confirmed.

In our previous XAS measurements, we have succeeded in obtaining the absorption peak of carbonyl group (-COOH) for 4-MBA. In this case, we observed two distinct features at 532 and 535 eV in the O K-edge region. These are assigned as due to the transition to the π^* orbital in the C=O double bond. Here, we observed a rather weak feature at 533 and 536 eV for cysteine, as shown in Fig. 1. We expect that these are the slightly shifted components, similarly assigned to the C=O double bond.

As a result, we could have established the measurement set up for the transmission mode for both 4-MBA and cysteine. We now plan to investigate a series of alkanethiol molecules to form self-assembled monolayer (SAM), and compared their behavior with 4-MBA and cysteine.

The next step should be the observation of the change in the orientation/conformation depending on the applied bias to the electrode (Au membrane). We expect that the precursor phenomena be proved more clearly.

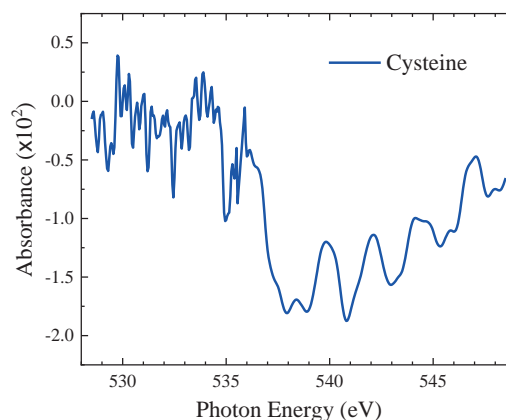


Fig. 1. O K-edge XAS spectrum for cysteine.

- [1] R. LeParc *et al.*, *Langmuir* **22** (2006) 3413.
- [2] C. I. Smith *et al.*, *J. Electrochem. Soc.* **150** (2003) 1.
- [3] N. Ikeda *et al.*, *ALC'19* (2019) 22.

Evaluation of Growth Orientation and Crystallinity of Deep UV Emitting Zinc Aluminate Thin Films

H. Kominami^{1,2,3}, K. Inoue¹, N. Uesugi¹, K. Nie¹, A. Adachi¹, R. Isihara¹, K. Yabe¹, J. Kamikawa², T. Sadamori², D. Takeya², N. Miyazaki², A. Dorokhina³ and S. Kurosawa^{4,5}

¹Graduate School of Integrated Science and Technology, Shizuoka University,

²Faculty of Engineering, Shizuoka University,

³Graduate School of Science and Technology, Shizuoka University,

¹⁻³3-5-1 Johoku, Naka-ku, Hamamatsu, 432-8651 Japan

⁴New Industry Creation Hatchery Center (NICHe), Tohoku University

6-6-10 Aza-Aoba, Aramaki, Aoba-ku, Sendai, Miyagi, 980-8579, Japan

⁵Faculty of science, Yamagata University, 1-4-12, Kojirakawa-machi, Yamagata, 990-8560, Japan

The UV light is used for various applications depending on the wavelength as well as the sterilization described above. Recently, from the viewpoint of consideration to the environment, the mercury free UV emission devices have been demanded for the application of catalyst and medical situations. In our previous work, it was clarified that ZnAl₂O₄ phosphor was suitable for the UV field emission lamp because of its stability and luminescent property. It shows strong UV emission peaked around 250 nm which suitable for sterilization.

In this research, ZnAl₂O₄ thin film layer were prepared by thermal diffusion of ZnO and sapphire substrate for new UV devices. In order to evaluate the inside of the film, an etching treatment was performed using hydrochloric acid.

XRD measurement was performed on the prepared sample. As a result, diffraction peaks of (220)(311)(400)(333) were observed. XRD measurement was performed on the prepared sample. As a result, diffraction peaks of (220)(311)(400)(333) were observed.

ϕ scan results of ZnAl₂O₄(220)(422)(533) and c-Al₂O₃ (110)(300) where diffraction peaks were observed in $2\theta/\phi$ scans around the a- and m-planes, a total of six diffraction peaks were observed every 60°. The results are shown in Fig.1. This is a diffraction peak with six-fold symmetry derived from α -Al₂O₃, which is a hexagonal system. ZnAl₂O₄ is a cubic substance, and ZnAl₂O₄ (220)(422)(533) also had a total of six diffraction peaks at intervals of 60°.

In ZnAl₂O₄{220}{422}, there are 6 planes perpendicular to ZnAl₂O₄ (333) every 60°. There is a face. From this, the diffraction peaks of ZnAl₂O₄ (220)(422)(533) with six-fold symmetry in the ϕ scan are considered to be the diffraction peaks of a crystal in which ZnAl₂O₄ (333) is oriented on the c-plane of c-Al₂O₃.

The six planes of ZnAl₂O₄{220} and {422} each form an angle of 30°, and the m-plane and a-plane of c-Al₂O₃ also form an angle of 30°. ZnAl₂O₄(220) and (422) are oriented along the m-plane and a-plane of c-Al₂O₃, respectively, from the measurement results of

$2\theta/\phi$ scans around the m-plane and a-plane of c-Al₂O₃, so ZnAl₂O₄{422} and the a-plane of c-Al₂O₃, and the m-plane of ZnAl₂O₄{220} and c-Al₂O₃ are parallel to each other.

From Fig.1, there is a large peak of 6-fold symmetry and a small peak of 6-fold symmetry at 30° shift (▼). In addition, ZnAl₂O₄(220) is also oriented on the a-plane of c-Al₂O₃ from the measurement result of $2\theta/\phi$ scan around the a-plane of c-Al₂O₃. These diffraction peaks are thought to be due to crystals formed by a phase relationship in which ZnAl₂O₄ is rotated 30° about ZnAl₂O₄[333], where the planes of ZnAl₂O₄ and c-Al₂O₃ are parallel to each other. Since almost no diffraction peaks other than the above two models are observed, it is considered that the sample is formed by the relationship between the phases of c-Al₂O₃ and ZnAl₂O₄ in these two models.

ϕ scans of ZnAl₂O₄(220) samples whose thin film surface was etched by hydrochloric acid showed that the sample etched about 400 nm lost some of its internal orientation, while the sample etched about 450 nm lost its orientation largely. lost part.

From the CL measurement results of this sample, the sample etched about 400 nm maintained the UV emission intensity, but then the emission intensity dropped sharply, and the sample etched about 450 nm did not obtain UV emission. From these results, it is considered that a uniform ZnAl₂O₄ thin film is formed from the sample surface to about 400 nm, but the formation of ZnAl₂O₄ is insufficient inside.

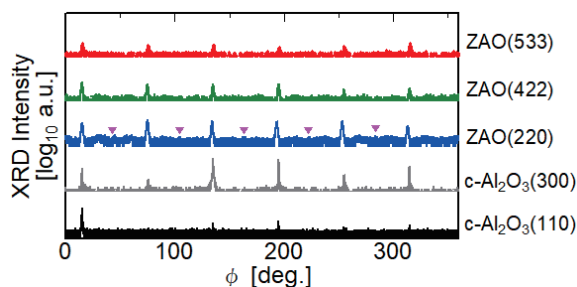


Fig. 1. ϕ - scan XRD spectra of ZnAl₂O₄ and c-Al₂O₃.

BL4U

Application of atomically-thin Graphene to X-ray Astronomy: Soft X-ray Transmission Measurements

I. Mitsuishi¹, K. Kashiwakura¹, Y. Niwa¹, T. Ogawa¹, M. Hirota¹, Y. Tawara¹, R. Kitaura²,
H. Yuzawa³, T. Ohigashi³ and K. Tanaka³

¹Graduate School of Science, Division of Particle and Astrophysical Science, Nagoya University, Furo-cho,
Chikusa-ku, Nagoya, Aichi 464-8602, Japan

²Department of Chemistry, Nagoya University, Nagoya 464-8602, Japan

³UVSOR Synchrotron Facility, Institute for Molecular Science, Okazaki 444-8585, Japan

Thin-film devices have been used in a large variety of fields including astronomy. In X-ray astronomy, thin-film devices have been prepared for payloads such as detectors and telescopes and playing a key role as, e.g., optical and contamination blocking filters and thermal shields [e.g., 1, 2]. For such thin film devices, severe launch and space environmental tolerance and high transmission are essential at the same time for high-sensitivity space observations in the limited observing time. Plastic films such as polyimide have often been adopted as thin films. However, there is still room for improvement especially in transmission of a soft energy range below 1 keV. Thus, we have proposed to make use of graphene which is an atomically-thin material but has excellent mechanical strength. Our idea is to apply graphene to thin film devices in X-ray astronomy [3].

As a first step, we conducted rough X-ray transmission measurements from 100 to 500 eV and confirmed very high transmission for both single- and five-layer graphene sample [3]. As a next step, we performed detailed X-ray transmission measurements to understand systematic errors for the observed values in this experimental setup and aging degradation as shown in Fig. 1. We used the same quartz substrates with large tapers with an angle of 30 degrees to avoid the shadowing effect by the substrate for focused X-ray photons by the Fresnel zone plate. Consequently, very high transmission, specifically 94-99% and 95-101% for single- and five-layer graphene samples in nominal values except the C K-edge structure, was obtained. The systematic errors are estimated to be 3% for our sample in this experimental setup considering short- and long-term time variability and spatial dependence and thus, there is no significant differences in the transmission between the samples within the systematic errors in our current experimental setup. This suggests that very high transmission is expected even for five-layer graphene films with much stronger mechanical strength which allows us to fabricate free-standing structures with larger diameter much easier. The results are shown in Fig. 2. We confirmed that there is no significant aging degradation at least for the single-layer graphene sample for 9 months. The paper including these results is being prepared (Kashiwakura, Mitsuishi *et al.*, in prep.).

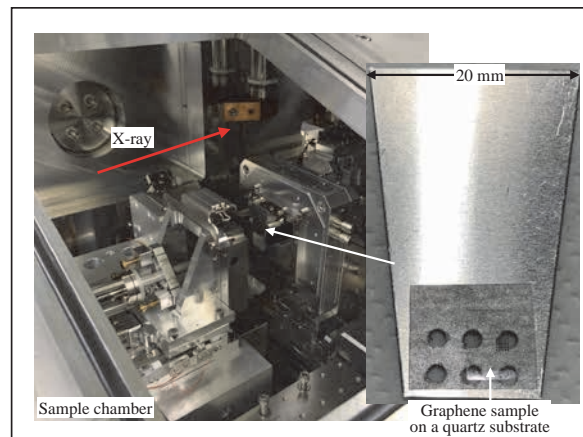


Fig. 1. Sample chamber and a close-up view of the graphene sample on the quartz substrate with a taper structure.

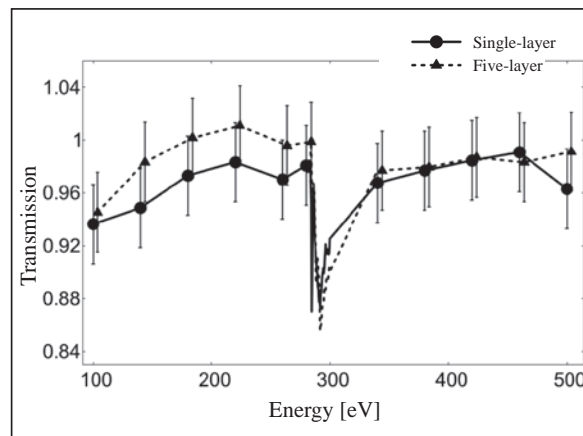


Fig. 2. Resultant transmission from 100 to 500 eV for single- (filled circle) and five-layer (triangle) graphene samples (Kashiwakura, Mitsuishi *et al.*, in prep.). Systematic errors are +/-3%.

- [1] P.J. Serlemitsos *et al.*, Publ. Astron. Soc. Japan **47** (1995) 105-114.
 [2] P.J. Serlemitsos *et al.*, Publ. Astron. Soc. Japan **59** (2007) S9-S21.
 [3] I. Mitsuishi *et al.*, UVSOR Activity Report 2021 **49** (2022) 45.

Tuning Magnetic Properties of Atomic Layer Materials by organic-inorganic Interfacial Magnetic Coupling

H. Ono¹, Y. Umeda¹, K. Yamamoto^{3,4}, O. Ishiyama^{3,4},
T. Yokoyama^{3,4}, M. Mizuguchi^{1,2} and T. Miyamachi^{1,2}

¹Department of Materials Science and Engineering, Nagoya University, Aichi, 464-8603, Japan.

²Institute of Materials and Systems for Sustainability (IMaSS), Nagoya University, Aichi, 464-8601, Japan.

³Institute for Molecular Science, Myodaiji-cho, Okazaki 444-8585, Japan

⁴The Graduate University for Advanced Studies, Myodaiji-cho, Okazaki 444-8585, Japan

Organic materials are expected to be useful to spintronics devices due to their low spin current dissipation derived from weak spin-orbit interaction. Organic-inorganic hybrid interface has been studied because of its controllable interfacial spin state via the proximity effect. Spin-dependent electron transport properties depend on the electronic interaction between organic and inorganic materials and local interface structures. Thus, understanding structural, electronic and magnetic properties of the organic-inorganic interface on the level of single molecules is important for realizing molecular spintronics devices. However, microscopic details of the hybrid interface have not been clarified so far.

In this study, we fabricate organic-inorganic hybrid films and investigate their intrinsic electronic and magnetic properties on the level of single molecules. For this purpose, ferromagnetic iron nitride atomic layers with γ' -Fe₄N stoichiometry were chosen as an inorganic material, which uniformly grow and show high surface quality on the atomic scale [1,2]. Molecular layers composed of planer cobalt phthalocyanine (CoPc) were chosen as an organic material. Structural, electronic and magnetic properties of the hybrid interface composed of CoPc with the thickness of 1, 2 and 3 molecular layers and a bilayer γ' -Fe₄N were investigated by scanning tunneling microscopy (STM), low energy electron diffraction (LEED) and x-ray absorption spectroscopy/magnetic circular dichroism (XAS/XMCD).

A bilayer γ' -Fe₄N was prepared by iron deposition on Cu (001) with N⁺ ion bombardment and subsequent annealing at 620 K. Then, CoPc/ γ' -Fe₄N hybrid thin films were fabricated by depositing CoPc on the γ' -Fe₄N at room temperature. In combination with results of STM and LEED, the impact of thickness-dependent structural properties of CoPc layers on the interfacial Fe and Co spin states were investigated by XMCD.

XAS/XMCD measurements were performed at BL4B in UVSOR by total electron yield mode at B = 0 ± 5 T and T = 7.3 K. The XMCD spectra are obtained at the normal (NI: $\theta = 0^\circ$) and the grazing (GI: $\theta = 55^\circ$) geometries by detecting $\mu_+ - \mu_-$, where μ_+ (μ_-) denotes the XAS recorded at Fe and Co L adsorption edges with the photon helicity parallel (antiparallel) to the sample magnetization. Note that θ is the angle between the sample normal and the incident x-ray [3].

We confirm the magnetic coupling for CoPc(1ML)/ γ' -Fe₄N from the finite of Co XMCD signal. The perpendicular magnetic anisotropy of γ' -Fe₄N, which is proportional to the difference between out-of-plane and in-plane Fe orbital magnetic moment obtained by XMCD sum rule, becomes larger after the deposition of CoPc molecules on the γ' -Fe₄N. This result indicates the magnetic coupling with CoPc enhances the perpendicular magnetic anisotropy of γ' -Fe₄N. As for magnetic properties of CoPc, we find that Co out-of-plane and in-plane XMCD signals show different behaviors with increasing the amount of CoPc. While the out-of-plane Co XMCD signal gradually decreases with increasing CoPc thickness, the strong Co XMCD is maintained in the in-plane direction. Taking the random stacking of CoPc layers revealed by STM and LEED, these results indicate that the orbital dependent magnetic coupling between CoPc layers, i.e., the magnetic coupling via the in-plane Co 3d orbitals is weak, but that via the out-of-plane Co 3d orbitals relatively robust.

[1] Y. Takahashi *et al.*, Phys. Rev. Lett. **116** (2016) 056802.

[2] Y. Takahashi *et al.*, Phys. Rev. B **95** (2017) 224417.

[3] S. Nakashima *et al.*, Adv. Funct. Mater. **29** (2019) 1804594.

[4] P. Bruno, Phys. Rev. B **39** (1989) 865.

BL4B (XMCD)

X-ray Magnetic Circular Dichroism Study of Chiral Antiferromagnetic $\text{Co}_{2-x}\text{Pd}_x\text{Mo}_3\text{N}$ Thin Films

B. Qiang^{1,2}, M. Togashi³, T. Fukasawa¹, T. Hajiri¹, M. Kuwahara^{3,4}, H. Asano^{1,5} and T. Ito⁶¹Department of Materials Physics, Nagoya University, Nagoya, Japan, 464-8603²Department of Materials Design Innovation Engineering, Nagoya University, Nagoya, Japan, 464-8603,³Department of Applied Physics, Nagoya University, Nagoya, Japan, 464-8603⁴Institute of Materials and Systems for Sustainability, Nagoya University, Nagoya, Japan, 464-8603⁵Research Department, Nagoya Industrial Science Research Institute, Nagoya, Japan, 464-0819⁶Synchrotron Radiation Research Center, Nagoya University, Nagoya, Japan, 464-8603

Dzyaloshinskii-Moriya (DM) interaction-induced magnetic skyrmions [1,2] have been observed in many chiral magnets with broken space reversal symmetry [3,4]. Recently, filled β -Mn-type $\text{Fe}_{2-x}\text{Pd}_x\text{Mo}_3\text{N}$ [5] and $\text{Co}_{2-x}\text{Pd}_x\text{Mo}_3\text{N}$ (CPMN) [6,7] have been reported to host small size skyrmions at room-temperature, which are a good playground for skyrmion device applications. X-ray magnetic circular dichroism (XMCD) is known as a very powerful tool to detect the element-specific spin and orbital states in each site. In this study, we have applied XMCD on filled β -Mn-type CPMN to elucidate the relation between its magnetism, especially ferromagnetic skyrmions at the low-temperature (Spiral-II) phase [6], and spin and orbital magnetic moment of Co.

CPMN ($x=1.01$) thin film (30 nm in thickness, without capping layer) was prepared using magnetron sputtering technique grown on C-sapphire substrates. Measurements of XAS/XMCD were performed at the BL4B in UVSOR by total electron yield mode at $T = 4$ K (Spiral-II phase). The external magnetic fields H up to ± 1 T were applied in parallel to the surface normal axis. The circularly polarized x-ray beam was induced nearly parallel to H . It should be noted that each $\text{Co } L_{2,3}$ XAS spectra at $H = +0.5 \sim +0.1$ T ($-0.5 \sim -0.1$ T) were obtained after the magnetization due to canted antiferromagnetism being saturated at $H = -1$ T ($+1$ T), since the magnetic skyrmions in this system is expected to be generated around $H = \pm 0.2$ T asymmetrically with respect to the zero field (see inset of Fig. 1(b))[6].

Figures 1(a) and 1(b) show the magnetic field dependence of the $\text{Co } L_{2,3}$ edge-XAS spectra of CPMN ($x = 1.01$) and the XMCD spectrum obtained by subtracting XAS spectra between $H = +1$ T ($\sim +0.1$ T) and $H = -1$ T (~ -0.1 T), respectively. It can be seen that a clear XMCD is observed at $H = \pm 1$ T, where the spin state associated with the formation of canted antiferromagnetism is expected from the magnetic and transport measurements at the low temperature region. With decreasing magnetic field, the observed XMCD intensity gradually decreases, and a opposite sign of the XMCD intensity near the L_3 edge at 778 eV appears in the region of $H < \pm 0.25$ T, where magnetic skyrmion

formation is expected from the topological Hall effect measurement (Fig. 1(b), inset). We expect that the observed magnetic field dependence of XMCD near the low-energy edge might suggest the change in the magnetic structure associated with the formation of magnetic skyrmions on CPMN.

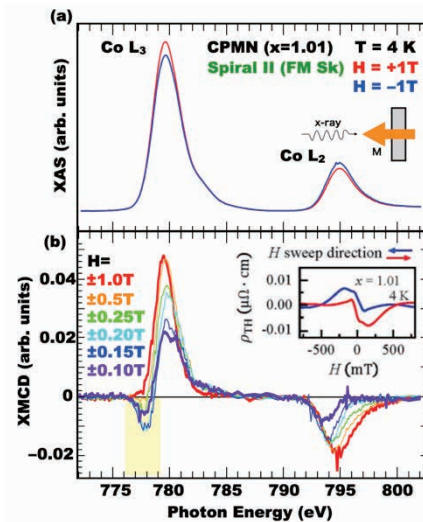


Fig. 1. (a) XAS spectrum at the $\text{Co } L_{2,3}$ edge obtained by using the photon helicity parallel (μ^+ , red) and antiparallel (μ^- , blue) to the external magnetic field H , respectively. (b) External magnetic field dependence of XMCD spectra ($\mu^+ - \mu^-$) for CPMN ($x=1.01$) at $T = 4$ K. Inset shows the field dependence of topological Hall effect [6].

[1]T. Jo, J. Phys. Soc. Jpn. **62** (1993) 1814.[2]Y. Teramura, A. Tanaka, and T. Jo, J. Phys. Soc. Jpn. **65** (1996) 1053.[3]C. Papas *et al.*, Phys. Rev. Lett. **102** (2009) 197202.[4]V. Kumar *et al.*, Phys Rev B **101** (2020) 014424.[5]B. W. Qiang *et al.*, Appl. Phys. Lett. **117** (2021) 142401.[6]B. W. Qiang *et al.*, Jpn. J. Appl. Phys. **61** (2022) 120901.[7]B. W. Qiang *et al.*, AIP Advances **13** (2023) 025138.

Controlling Magnetic Anisotropy of Magnetic Thin Film Heterostructures

Y. Umeda¹, H. Ono¹, K. Yamamoto^{3,4}, O. Ishiyama^{3,4},
T. Yokoyama^{3,4}, M. Mizuguchi^{1,2} and T. Miyamachi^{1,2}

¹Department of Materials Science and Engineering, Nagoya University, Aichi, 464-8603, Japan.

²Institute of Materials and Systems for Sustainability (IMaSS), Nagoya University, Aichi, 464-8601, Japan.

³Institute for Molecular Science, Myodaiji-cho, Okazaki 444-8585, Japan

⁴The Graduate University for Advanced Studies, Myodaiji-cho, Okazaki 444-8585, Japan

3d transition metal ordered alloy thin films with L1₀ crystal structure are attracting attention as rare-earth free magnetic materials due to their large perpendicular magnetic anisotropy, large magnetic moment, and high Curie temperature. Using pulsed laser deposition, the growth of FeCo thin films with alternating Fe and Co atomic layers was investigated [1]. Although much effort has been made to realize uniaxial anisotropy in the L1₀-FeCo phase, the L1₀ structure is a non-equilibrium state of the FeCo phase and hence the method for achieving the out-of-plane magnetization has not been established. The main problem could be caused by atomic-scale disorder at the Fe/Co interface during growth processes, which highlights the importance of microscopic characterizations of the structural, electronic, and magnetic properties of L1₀-FeCo. Therefore, we intend to fabricate high-quality FeCo alloy thin films on Cu(001) substrates by utilizing the nitrogen surfactant effect of a monatomic layer nitride. The high surface lattice stability of a monatomic layer nitride and the nitrogen surfactant effect that effectively suppresses the interdiffusion at the heterointerface could lead to the growth of FeCo alloy thin films with atomically flat and uniform interfaces [2,3]. The important role of the nitrogen surfactant effect in the preparation of high-quality L1₀-type alloy thin films has been demonstrated for FeNi alloy thin films [2].

In this study, FeCo ordered alloy thin films in the initial growth stage were prepared using the nitrogen surfactant effect. The correlation between the structural changes at the FeCo interface and magnetic properties upon sample heat treatment was investigated using low-energy electron diffraction (LEED) and X-ray absorption spectroscopy/X-ray magnetic circular dichroism (XAS/XMCD). FeCo alloy multilayer thin films were grown on Cu(001) using the following process: (1) a bilayer iron nitride (Fe₂N/Fe) was first grown on Cu(001), (2) 1 monolayer (ML) of Co was deposited at a low temperature (~150 K), (3) annealing was carried out at 300, 570, and 670 K, and (4)

additional 1 ML of Fe was deposited at a low temperature (~150 K) for samples heated at 570 K (FeN/Co/Fe/Fe). The annealing temperature dependence of electronic and magnetic properties was investigated by XAS/XMCD. XAS/XMCD measurements were performed at BL4B in UVSOR by total electron yield mode at $B = 0 - \pm 5$ T and $T = 7.9$ K. The XMCD spectra are obtained at the normal (NI: $\theta = 0^\circ$) and the grazing (GI: $\theta = 55^\circ$) geometries. Note that θ is the angle between the sample normal and the incident x-ray. Element specific magnetization curves were also recorded by plotting the L₃/L₂ Fe and Co XAS intensities as a function of the magnetic field.

The XMCD signal of the bilayer iron nitride is greater in the GI geometry than in the NI geometry, revealing its strong in-plane magnetic anisotropy as previously reported [3]. Adding 1 ML Co activates the nitrogen surfactant effect [2], which leads to the formation of CoN in the topmost layer (CoN/Fe/Fe). Accordingly, we observed an increase in the out-of-plane magnetization of the Fe layer from Fe magnetization curves. The perpendicular magnetic anisotropy of the Fe layer is further enhanced by annealing at 570 K. However, at an annealing temperature of 670 K, a decrease in the coercivity of the Fe layer is observed. Taking into consideration the annealing temperature dependence of the LEED pattern, the enhancement of the out-of-plane magnetization could be due to improved ordering of the Co/Fe interface up to annealing temperatures of 570 K. At 670 K, surface N atoms start to desorb, which induces the interdiffusion of interfacial Co and Fe atoms and consequently lowers the coercivity. In the sample with additional Fe layers (FeN/Co/Fe/Fe), the perpendicular magnetic anisotropy of Fe is further enhanced.

[1] H. Ito *et al.*, AIP Adv. **9** (2019) 045307.

[2] K. Kawaguchi *et al.*, Phys. Rev. Mater. **4** (2020) 054403.

[3] Y. Takahashi *et al.*, Phys. Rev. B **95** (2017) 224417.

BL4B

X-ray Photoemission Spectroscopy and X-ray Absorption Spectroscopy Measurement of the Chiral Molecule on the Metal Substrate

F. Nishino^{1,2}, K. Fukutani^{1,2}, P. I. Jaseela^{1,2}, H. Iwayama^{1,3}, S. Makita³ and S. Kera^{1,2,3,4}

¹Institute for Molecular Science, Okazaki 444-8585, Japan

²The Graduate University for Advanced Studies (SOKENDAI), Okazaki 444-8585, Japan

³UVSOR Synchrotron Facility, Institute for Molecular Science, Okazaki 444-8585, Japan

⁴Graduate School of Science and Engineering, Chiba University, Chiba 263-8522, Japan

Chirality-induced spin selectivity (CISS) is a phenomenon in which the spin of an electron is polarized/filtered in the process of electron transfer (transmission) in a system with broken mirror symmetry. The spin polarization by chiral molecular CISS in the gas phase was studied from 1980's. Since it was reported that the spin polarization was less than 0.5%, CISS has not attracted wide attention at this time. However, in 1999, R. Naaman *et al.* reported that spin-unpolarized electrons that transmitted through the chiral molecular film on solids exhibited spin polarization as high as 60% at room temperature [1]. While the CISS does not require magnetic materials or external magnetic fields, it exhibits higher spin polarization than the spin filters using magnetic metals. These features are expected to be applied to magnetic storage media with high storage density. Therefore, CISS by organic chiral molecules has been actively studied both theoretically and experimentally to elucidate its mechanism and for the purpose of device applications. Presently, however, the details of mechanism why chiral molecular film on solid exhibits spin polarization larger than 1000 times that of gas-phase molecules remains unsolved. For this reason, the gap between the theory and the application research is growing. In order to elucidate the mechanism, it is necessary to rigorously observe the interaction between the travelling electrons and the chiral molecules. In order to understand the CISS processes in chiral molecules, it is important to investigate how CISS effect depends on the relative orientations among the chiral molecules, the substrate, and the direction of electron transmission. Also, the difference of electronic structure and structure between the gas phase and the chiral molecular film on substrate.

In this study, the chiral molecule 2,2'-Bis(diphenylphosphino)-1,1'-binaphthyl (BINAP hereafter) shown in Fig. 1(a) were deposited on a clean Au(111) substrate, and *in-situ* X-ray photoemission spectroscopy (XPS) measurements were performed to investigate the interactions between BINAP molecules and Au(111) substrate.

Figure 1(b) shows the results of XPS from the phosphorus (P) 2*p* core orbital of BINAP molecules, acquired at the nominal coverages of 0.4 monolayer (ML) and 2 ML of (*R*)-BINAP on Au(111).

Interestingly, while the molecules at the sub-

monolayer coverage (0.4 ML) are expected to interact more strongly with the substrate than the multi-layer coverage (2 ML), we find that the P2*p* core peaks appear very similar, as can be seen from the peak fitting results for the two peaks [labelled A and B in Fig. 1(b)]. This likely signifies that the intermolecular interactions are much stronger (which determines the chemical shift of the atomic orbitals) than the molecule-substrate interactions. This view is indeed consistent with the later measurements in our project using the low-energy electron diffraction (LEED) and scanning tunnelling microscopy (STM), which clearly reveals the weakly-interacting incommensurate molecular overlayer structures.

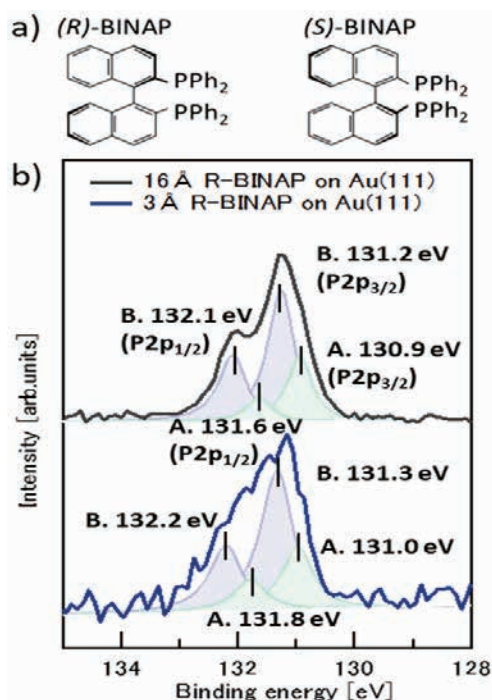


Fig. 1. (a) Molecular structures of (*R*)- and (*S*)-BINAPs. (b) P2*p* core level peaks of (*R*)-BINAP on Au(111) measured by XPS at the nominal coverages of 0.4 ML (bottom) and 2 ML (top). The spectra at each coverage are fitted with the two spin-orbit doublets [labelled A (green) and B (blue)] with Doniach-Sanjic lineshape.

[1] K. Ray, S. P. Ananthavel, D. H. Waldeck and R. Naaman, *Science* **283** (1999) 814.

Observation of Heat Treatment Effects of Amorphous Selenium Thin Film by Vacuum Ultraviolet Transmission Spectrum

K. Hayashi

Department of Electrical, Electronic and Computer Engineering, Gifu University, Gifu 501-1193, Japan

It is well-known that various photoinduced phenomena [1,2] such as changes in optical band gap, conductivity, and volume occur in chalcogenide amorphous semiconductors by light irradiation. Although many studies have been done on the photoinduced phenomena of these materials, little is known about the details of these mechanisms. These phenomena were studied by exciting outer core electrons with the irradiation of light with the energy corresponding to the optical bandgap or sub-bandgap. The interest has been attracted for the change of the optical properties in the energy region of the visible light. We are interesting for the changes of the optical properties in the higher energy region. To obtain a wide knowledge of the photoinduced phenomena, it is necessary to investigate to the photoinduced and heat treatment effects on wide energy region. In this report, we report heat treatment effects on the vacuum ultraviolet (VUV) transmission spectra of amorphous selenium thin film.

Sample used for the measurement of the VUV transmission spectra was amorphous selenium thin film prepared onto thin aluminum film by conventional evaporation technique. The sample thickness was about 180nm. The aluminum film of the thickness of 200 nm was used to eliminate the higher order light from the monochromator in the VUV region. These measurements were carried out at room temperature on the BL4B beam line of UVSOR. The spectrum was measured by using the silicon photodiode as a detector. Two pinholes of 1.5mm in a diameter were inserted between the monochromator and sample to remove stray light. The intensity of the VUV light was monitored by measuring the TPEY of a gold mesh. The positions of the core levels for the samples were calibrated by referencing to the 2p core level absorption of the aluminum film. Observation of the heat treatment effect in the VUV transmission spectrum was carried out by performing heat treatment for one hour at each temperature up to 363K.

Figure 1 shows heat treatment effects on the VUV transmission spectrum of an amorphous selenium thin film. Main absorption peaks around 22nm corresponds to the 3d core level of Se atom. The absorption spectrum observed in the amorphous selenium thin film is roughly consistent with the previous report [3]. Although the spin-orbit splitting of the 3d_{5/2} and 3d_{3/2} level of Se atom is not clearly resolved in this amorphous selenium thin film. I don't know the cause, but there may be differences in the preparation

conditions of the film. As can be seen from the figure, a significant change in the VUV transmission spectrum is observed by heat treatment at temperatures above 343K. We are also studying the effect of heat treatment on the photoconductivity of amorphous selenium thin films in our laboratory. There is a correlation between the heat treatment effect on photoconductivity and VUV transmission spectrum, and it is thought that this change is due to the crystallization of the amorphous selenium thin film. From the VUV transmission spectrum change of selenium thin films by heat treatment, it can be seen that the broad peak around 20nm in the VUV transmission spectrum of amorphous selenium thin films is composed of about three absorption peaks. It is not clear about the origin of broad spectra and several peaks. I think that these origins are related to the local structures of the amorphous network. The detailed experiments and analysis will be done in the next step. More detailed experiments are necessary to clarify the origin of the VUV transmission spectra.

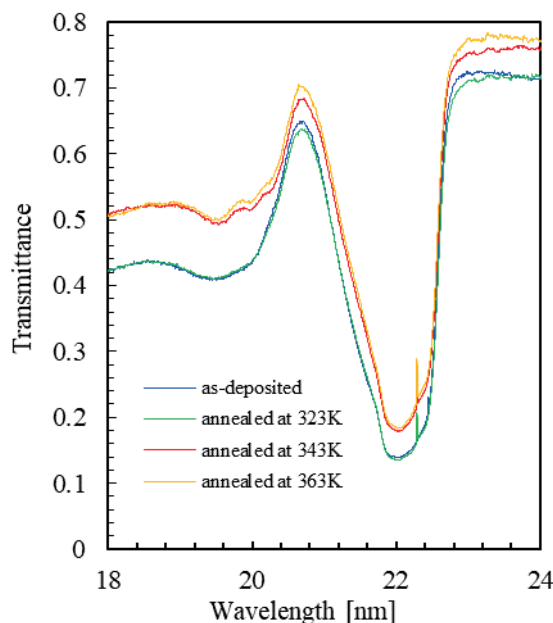


Fig. 1. Heat treatment effects on the VUV transmission spectrum of amorphous selenium film.

- [1] K. Tanaka, *Rev. Solid State Sci.* **4** (1990) 641.
- [2] K. Shimakawa, S. Inami, and S. R. Elliott, *Phys. Rev. B*, **42** (1990) 11857.
- [3] J. Bordas and J. B. West, *Phil. Mag.* **34** (1976) 501.

BL4B

UV-X-ray Transmission Measurements of Atomically Thin Graphene Astronomical Applications

I. Mitsuishi¹, K. Kashiwakura¹, Y. Niwa¹, T. Ogawa¹, R. Kitaura², E. Nakamura³,
M. Nagasaka³ and K. Tanaka³

¹Graduate School of Science, Division of Particle and Astrophysical Science, Nagoya University, Furo-cho,
Chikusa-ku, Nagoya, Aichi 464-8602, Japan

²Department of Chemistry, Nagoya University, Nagoya 464-8602, Japan

³UVSOR Synchrotron Facility, Institute for Molecular Science, Okazaki 444-8585, Japan

Thin-film devices have been utilized in a great variety of uses as not only ground-based but also space-based applications such as optical and contamination blocking filters and thermal shields [e.g., 1, 2]. Recently, polyimide films have often been used as thin films considering relatively stronger mechanical strength in plastic films. However, there is still room of improvement in sensitivity of the thin films (= transmission) below 1 keV including UV region although such energy ranges are very informative for understanding, e.g., stellar coronae and large-scale structure of the Universe [e.g., 3, 4]. Thus, we have proposed to make use of graphene which is an atomically-thin material but has excellent mechanical strength. Our idea is to apply graphene to thin film devices in X-ray astronomy [5].

As a first step, we measured reflectivity at a soft X-ray range between 100 and 500 eV successfully for single- and five-layer graphene samples at BL4U and confirmed very high transmission above 90% except C K-edge structure [5]. Thus, as a next step, we tried to measure transmission in UV region below 100 eV and construct our original experimental setup at BL4B. Our experimental setup is shown in Fig. 1 and we prepared a five-layer graphene sample with a diameter of 300 μm on a quartz substrate to obtain larger photon statistics. To check the consistency of transmission between the beamlines of BL4U and BL4B, we used the same sample and measured transmission from 100 to 250 eV as well. Consequently, we measured transmission from 30 to 100 eV successfully and confirmed very high transmission from 91 to 101% in nominal values with systematic errors of 5% due to short- and long-term time variability. We confirmed that there are no significant differences in 100-250 eV between the results obtained from BL4B and BL4U. The results are summarized in Fig. 2. A slight decreasing trend can be seen toward 30 eV even though the systematic errors are high (5%). This trend is the same as the expected from a database for bulk carbon. In order to verify the trend, we need additional measurements with smaller measurement accuracy of <2% down to 10 eV. The paper including these results is being prepared (Kashiwakura, Mitsuishi *et al.*, in prep.).

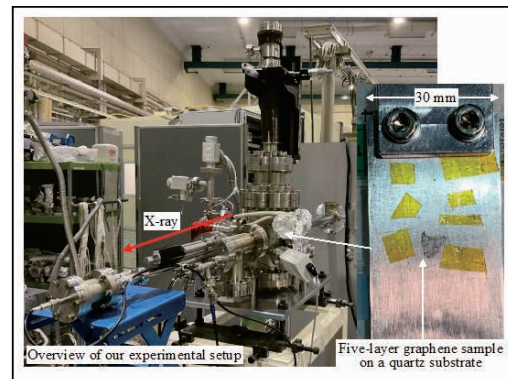


Fig. 1. Sample chamber and a close-up view of the graphene sample on the quartz substrate.

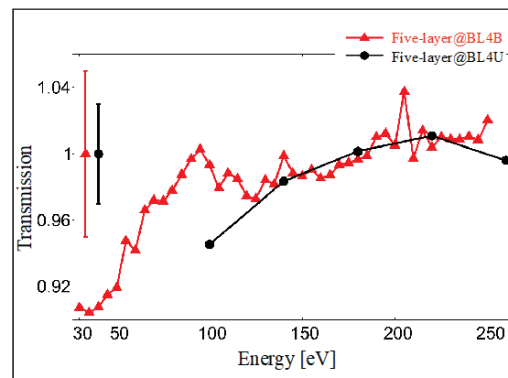


Fig. 2. Resultant transmission from 30 to 250 and from 100 to 250 eV for five-layer graphene samples measured at BL4B (filled triangle) and BL4U (filled circle) (Kashiwakura, Mitsuishi *et al.*, in prep.). Systematic errors are 5% / 3% at BL4B / BL4U.

- [1] P.J. Serlemijos *et al.*, Publ. Astron. Soc. Japan **47** (1995) 105.
- [2] P.J. Serlemijos *et al.*, Publ. Astron. Soc. Japan **59** (2007) S9.
- [3] I. Mitsuishi *et al.*, Publ. Astron. Soc. Japan **64** (2012) 18-1.
- [4] S. Takasao, I. Mitsuishi *et al.*, The Astrophys. J. **901** (2020) 70.
- [5] I. Mitsuishi *et al.*, UVSOR Activity Report 2021 **49** (2022) 45.

Si *L*-edge NEXAFS Spectra of Native Oxide Si Wafer with Different Crystal Surface

K. K. Okudaira¹, S. Yoshioka² and E. Kobayashi³

¹Graduate School of Engineering, Chiba University, 1-33 Yahooi-cho, Inage-ku Chiba 263-8522, Japan

²Graduate School of Engineering, Kyushu University, 744 Motoooka Nishi-ku Fukuoka 819-0395 Japan

³Kyushu Synchrotron Light Research Center, 8-7 Yayoigaoka, Tosu, Saga 841-0005, Japan

Silicon dioxide is one of the most popular substrate for inorganic semiconductor devices as well as organic devices such as self-assembled monolayers, which is useful for organic field effect transistors. [1] One important advantage of the silicon substrate over the metal substrate is that conductive currents are eliminated. The leakage current is relatively large by using native oxide Si wafer as dielectric layer due to the thinness and inhomogeneous of oxide layer of native oxide Si wafer. The application of self-assembled monolayer to SiO₂/Si substrate depress the leakage current. [2] The electrical properties such as insulation characteristics depends on the structure of surface silicon dioxides layer, which is considered amorphous. It is expected that the properties of native oxide layer on Si substrates would be affected by the underlying crystalline Si.

In this report, we investigate the effect of crystal structure of underlying crystalline Si on the surface structure of silicon dioxide by means of NEXAFS of native oxide Si(001) and Si(111) wafers.

NEXAFS spectra of the native oxide Si(001) and Si(111) wafers were measured at the beamline 4B of the UVSOR in the Institute of Molecular Science. In the total electron yield (TEY), the drain current of the sample was measured. All experiments were performed at room temperature.

Figure 1 shows the TEY Si *L*_{2,3} edge NEXAFS spectra of native oxide of Si(111) and Si(001) wafers. In the observed fine structure two region are identified. The absorption features observed from 100 to 104 eV are attributable to Si⁰ (crystalline Si under native oxide layer) and those from 104 to 110 eV are associated with Si⁴⁺ (SiO₂) [3]

In the hv range from 100 eV to 104 eV due to the Si crystalline layer, the spectral structure of Si(001) is identical with the one of Si(111). On the contrary, the spectral feature of native SiO₂/Si(001) is different from that of SiO₂/Si(111) in the hv range from 104 to 110 eV,

which is attributed to native oxide layer (SiO₂). By closed comparison the relative intensity of the peak a₁ at hv of 106 eV to that of the peak a₂ at hv of 106.8 eV for the SiO₂/Si(001) is different from that of SiO₂/Si(111). The peak a₁ disappears in the observed Si *L*-edge NEXAFS of native oxides Si(111) wafer. The peaks a₁ and a₂ can be assigned to 2p_{3/2} and 2p_{1/2} → the antibonding orbital of Si 3s character. [4] Harp *et al.* shows the peak positions of a₁ and a₂ depend on not only the oxidation state but also the thickness of native oxide layer [5]. These differences indicate that the properties of surface native oxide layer such as bonding structure as well as oxidation states are affected by underlying crystalline Si layer.

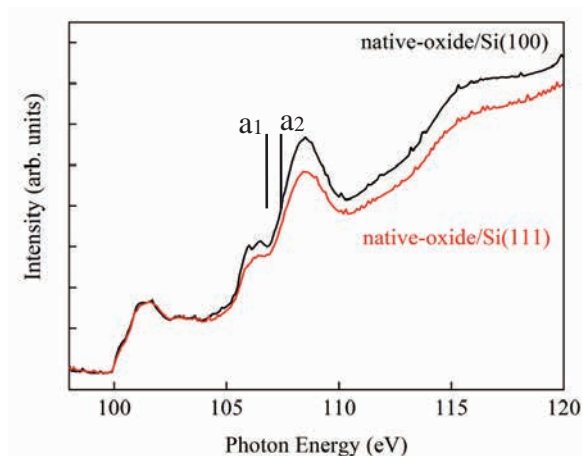


Fig. 1. Si *L*-edge NEXAFS of native oxide Si(001) and Si(111) wafers in TEY mode

[1] M. McDowell *et al.*, Appl. Phys. Lett. **88** (2006) 073505.

[2] M. -H. Yoon *et al.*, PNAS **102** (2005) 4678.

[3] M. Kasrai *et al.*, Appl. Surf. Sci., **99** (1996) 303

[4] M. Kasrai *et al.*, J. Vac. Sci. Tech. **A11** (1993) 2694.

[5] G. R. Harp *et al.*, J. Vac. Sci. Tech. **A8** (1990) 2566.

BL5U

ARPES from $\text{Si}\{111\}\sqrt{3} \times \sqrt{3}$ -Ag ultra-thin Film on Artificially Designed three-dimensional Si facet-line Structure with $\{111\}$ Facet Surfaces on $\text{Si}(001)$ Substrates

K. Hattori¹, Ni'matil Mabarroh¹, Juharni¹, Y. Ida¹, W. Imayama¹, Y. Kimoto¹, Y. Kitagawa¹, S. Tanaka², A. N. Hattori², S. Suga² and K. Tanaka³

¹Nara Institute of Science and Technology, Ikoma 630-0192, Japan

²SANKEN, Osaka University, Ibaraki, 567-0047, Japan

³UVSOR Synchrotron Facility, Institute for Molecular Science, Okazaki 444-8585, Japan

Highly densified device like 3D FET has been required by information society to break the limitation of miniaturizing 2D planar-type devices. Control of 3D structure device is indispensable to improve the specification, such as carrier mobilities on any direction surfaces of the 3D structures.

Recently, our group has successfully created 3D-Si surfaces by combining lithography and surface treatment techniques [1-4], and reported a successful creation of $\text{Si}\{111\} 7 \times 7$ clean facet surfaces showing surface and bulk electronic bands on $\text{Si}(110)$ substrates using laboratory based angle-resolved photoelectron spectroscopy (ARPES) [5], aiming for a future 3D-surface band-engineering. Here, we first demonstrated the creation of ultra-thin film on 3D Si clean facet surfaces indicating characteristic film band structures, essential for the 3D surface control.

In our experiment, 3D Si facet-lined structures with (111) and $(\bar{1}\bar{1}1)$ facet surfaces and $[\bar{1}10]$ -direction face edges on (001) substrates with the facet pitch of $4 \mu\text{m}$ period, were prepared by using a photo-lithography and wet etching (Fig. 1). After degassing and flashing the sample in ultra-high vacuum, $\{111\} 7 \times 7$ reconstruction was confirmed by low-energy electron diffraction (LEED). Subsequently Ag was deposited on the sample at $\sim 770 \text{ K}$, showing $\sqrt{3} \times \sqrt{3}$ reconstruction in both

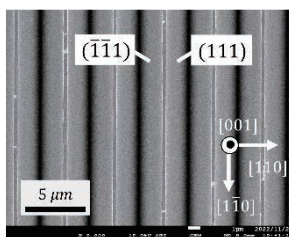


Fig. 1. SEM image of 3D Si facet-lined structure.

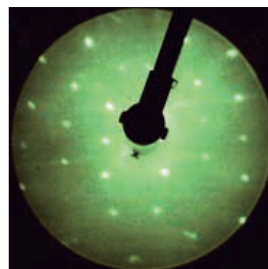


Fig. 2. LEED pattern of $\{111\}\sqrt{3} \times \sqrt{3}$ -Ag facet surfaces (120 eV).

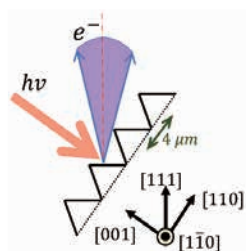


Fig. 3. ARPES geometry. 60 eV photons (pink) result in electron emission (purple) from (111) facet surfaces.

(111) and $(\bar{1}\bar{1}1)$ facet surfaces. Note that the superposition of the LEED patterns from the two facet surfaces are seen in Fig. 2.

ARPES was also performed in UVSOR at BL5U. Valence band dispersion was measured mainly at 70 eV photons with the (111) facet surface normal to the analyzer at 6 K, by optimizing the sample orientation (Fig. 3). We obtained the specific band structures caused by $\sqrt{3} \times \sqrt{3}$ -Ag ultra-thin film on the (111) facet surface (Figs. 4a and 4c), which was almost the same as those of the $\sqrt{3} \times \sqrt{3}$ -Ag on a 2D planar surface (Figs. 4b and 4d) measured under the same condition.

We confirmed that ARPES under optimizing 3D geometries informs us band structures of artificially designed 3D structure surfaces and “created films”. This will shed the light on future band engineering of 3D devices.

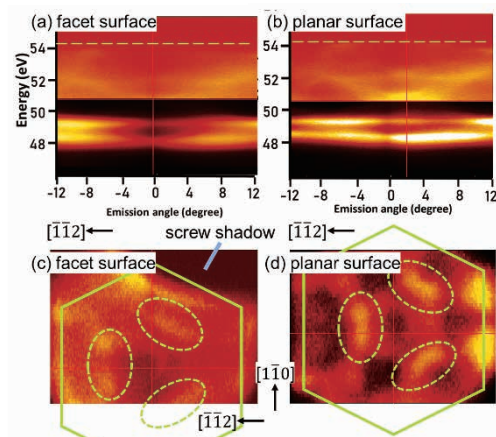


Fig. 4. E - k along $[\bar{1}\bar{1}2]$ (a, b) and k_x - k_y near Fermi level (dashed lines in a and b) (c, d) for facet (a, c) and planar (b, d) $(111)\sqrt{3} \times \sqrt{3}$ -Ag surfaces.

[1] A.N. Hattori, K. Hattori, *et al.*, Surf. Sci. **644** (2016) 86.

[2] A.N. Hattori, K. Hattori, *et al.*, Appl. Phys. Express **9** (2016) 085501.

[3] A.N. Hattori and K. Hattori, *21st Century Surface Science* (IntechOpen, London, 2020).

[4] S. Nakatsuka, T. Abukawa, A.N. Hattori, K. Hattori, *et al.*, e-J. Surf. Sci. NanoTechnol. **19** (2021) 13.

[5] K. Hattori, A. N. Hattori, *et al.*, e-J. Surf. Sci. Nanotechnol. **30** (2022) 214.

Sizable Rigid Shift of the Valence Band of h-BN by Cs-doping

S. Ichinokura¹, A. Hemmi², H. Cun², K. Tanaka³, T. Greber² and T. Hirahara¹

¹Department of Physics, Tokyo Institute of Technology, Tokyo 152-8551, Japan

²Physik-Institut, Universität Zürich, Winterthurerstrasse, 190, Zürich CH-8057, Switzerland

³UVSOR Facility, Institute for Molecular Science, Okazaki 444-8585, Japan

Hexagonal boron nitride (h-BN) is a two-dimensional semiconductor with a wide bandgap. Its gap size of around 5.9 eV corresponds to deep ultraviolet light, making h-BN a promising material for the development of energy-efficient optical disinfection devices. To reduce the working voltage of electroluminescence through tunneling carrier injection, it is required to develop p- and n-doping near the electrodes. However, the wide gap in h-BN poses a challenge for carrier doping through conventional substitution methods, which limits its use in electroluminescence devices.

To address this challenge, we are exploring an alternative approach known as chemical gating, which involves surface adsorption or intercalation of alkali metals (AMs) to the substrate interface. This creates an electrical dipole by facilitating charge transfer from the AMs to the substrate. Cs-doping has been shown to induce the largest electron doping in h-BN/Ir, where the valence band maximum (VBM), specifically the top of the π band at the K point, was indirectly estimated to be at 5.9 eV from the shift of the σ band at the Γ point, assuming a rigid band shift [1]. However, the limits of doping remain unclear until the direct observation of the band structure in a wide wavenumber range from Γ to K point.

In the present study [2], we conducted an analysis of the complete valence band structure of monolayer h-BN on Rh substrate before and after Cs doping via angle-resolved photoemission spectroscopy (ARPES) utilizing synchrotron radiation as a light source. The h-BN/Rh was grown by means of chemical vapor deposition. The doping of Cs was carried out via vacuum deposition at room temperature in the preparation chamber of the BL5U end station, followed by *in-situ* measurements of ARPES utilizing linear polarized light with $h\nu = 72$ eV at 200 K. Figures 1(a) and (b) depict the valence band spectra before and after Cs doping obtained by horizontally polarized (H-pol.) light, respectively, whereas Figures 1(c) and (d) show the same as Figs. 1(a) and (b), respectively, obtained by vertically polarized (V-pol.) light. The uppermost portion of the π band is located at the K point with a higher binding energy than the top of the σ band at the Γ point, making it possible for us to evaluate the VBM. E_{VBM} and E'_{VBM} are defined as the binding energy of the VBM before and after doping, as denoted by dashed black lines. The shift of the VBM, $\Delta E = E'_{\text{VBM}} - E_{\text{VBM}}$ is

observable to be 2.5 eV, identical to the σ band at the Γ point (refer to Figs. 1(c) and (d)). This clearly suggests a rigid shift of both the π and σ bands. Notably, Cs doping lowers the VBM to 5.7 eV. Considering the bandgap of h-BN is known to be 5.9 eV, the conduction band should lie only 0.2 eV above the Fermi surface. Thus, h-BN experiences significant electron doping.

As a concluding remark, for both Rh and Ir substrates, the VBM attained binding energy nearly equated to the band gap. This can be elucidated by the vacuum level alignment model when Cs is adsorbed on both sides of h-BN. This indicates that Cs with the lowest work function is the most efficacious, and this method can be implemented on an electroluminescence device using h-BN with any electrode.

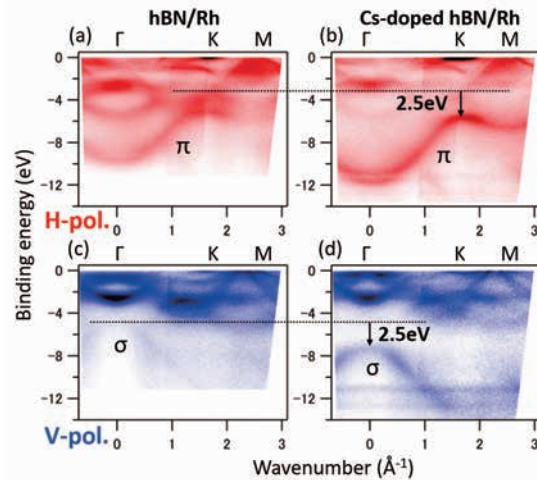


Fig. 1. ARPES spectrum of hBN along Γ -K-M line in the Brillouin zone. Panels (a) and (c) display the spectrum before Cs-deposition, while (b) and (d) show the spectrum after Cs-deposition. The spectra were obtained with $h\nu = 72$ eV at a temperature of 200 K. Panels (a) and (b) were obtained with horizontally-polarized light, while panels (c) and (d) were obtained with vertically-polarized light. In panels (a) and (b), the shift of VBM is indicated by black dashed line and arrow. In panels (c) and (d), the shift of σ band is denoted by black dashed line and arrow.

[1] J. Cai *et al.*, Phys. Rev. B **98** (2018) 195443.

[2] S. Ichinokura *et al.*, Appl. Phys. Lett. **122** (2023) 071601.

BL5U

Growth of Transition Metal Phosphide Thin Film on Au(111)

N. Maejima^{1,2}, K. Inaoka¹ and K. Edamoto^{1,2}

¹Coll. Sci., Rikkyo Univ., Tokyo 171-8501, Japan

²Research Center for Smart Molecules, Rikkyo Univ., Tokyo 171-8501, Japan

The Ni₁₂P₅@Au core-shell catalyst has attracted attention because of its high catalytic activity for oxygen evolution reactions [1]. Novel functions of core-shell catalysts arise from the interaction between the core and the shell at the interface [2]. Direct observation of the electronic states formed through the interactions between core and shell is difficult, and thus the fabrication of the Ni phosphide thin film on an Au substrate is desirable as a model system that allows the investigation using photoelectron spectroscopy. In this report, we will show that a nickel phosphide thin film can be grown on Au(111) by Ni deposition on a P-covered Au(111).

Experiments were performed at BL5U of the UVSOR facility. The Au(111) surface was cleaned by cycles of Ar⁺ ion sputtering (0.5 keV) and annealing (750 °C). P atoms were deposited on the Au(111) surface at 400°C (AuP/Au(111)). The prepared Au(111) and AuP/Au(111) samples showed 1x1 and 5x5 LEED patterns, respectively. Ni was subsequently evaporated onto AuP/Au(111) at 400°C to form a Ni_xP thin film on Au(111)(Ni_xP/Au(111)). This LEED pattern of this sample consisted of 1x1 spots arising from the Au(111) substrate and the additional 12 spots which are assigned as the spots from the Ni_xP crystal thin film. Au 4f, P 2p, Ni 3p and valence band photoelectron spectroscopy (PES) measurements were performed by an MBS A-1 analyzer. The ratio of the amount of Ni and P atoms on the Au substrate were determined by the ratios of the peak areas of Ni 3p and P 2p photoelectron spectra to be Ni : P = 2:1.

Au 4f_{7/2} spectra obtained from Au(111) clean surface, AuP/Au(111), and NiP/Au(111) samples are shown in Fig. 1. In the Au 4f_{7/2} spectra of Au(111) clean surface, two bulk and surface components were observed at binding energies of 84.0 and 83.7 eV, respectively.[3] The spectrum obtained from P deposited sample contain the bulk and surface Au-P component at 84.0 eV and 84.4 eV, respectively.[4] The surface component observed in the spectra of Au(111) clean surface has disappeared, indicating that the whole surface is covered with P. In the spectrum of the Ni deposited sample, peaks of bulk and surface components were observed at 84.0 eV and 83.7 eV, respectively. The disappearance of the peak at 84.4 eV corresponding to Au-P bonds indicates the cleavage of all Au-P bonds.

Though the P 2p spectrum obtained from Ni_xP/Au(111) contains multiple peak components, the component that is ascribed to P atoms bonded to Au was disappeared. In addition, the surface component observed in the spectrum of the Au(111) clean surface reappears in the spectrum of Ni_xP/Au(111). These results imply that the interaction between the thin film and the substrate is weak or the nickel phosphide film congregates to form islands. The Ni 3p peak position in the spectrum of Ni_xP/Au(111) was higher than that obtained from Ni₂P(10-10) single crystal by 0.3 eV [5], whereas the spectral shape was almost the same. These results suggested that a Ni phosphide whose composition was Ni : P = 2:1 can be formed on Au(111).

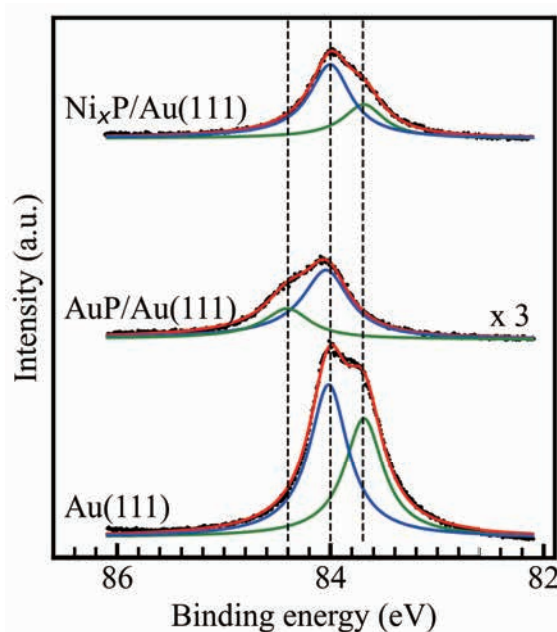


Fig. 1. Au 4f_{7/2} photoelectron spectra of clean Au(111), AuP/Au(111) and NiP/Au(111) samples.

- [1]Lee, Jong-Soo *et al.*, JACS **130** (2008) 9673.
- [2]Xu, Yingying *et al.*, Nano research **10** (2017) 3103.
- [3]Citrin, Ph. H. *et al.*, Phys. Rev. Lett. **41** (1978) 1425.
- [4]Zhang, Wei *et al.*, Small **14** (2018) 1804066.
- [5]N. Maejima *et al.*, UVSOR Activity Report **48** (2020) 115.

Heavy-Fermion in a Mono-Atomic Layer YbCu₂/Cu(111)

H. Sugihara¹, T. Nakamura^{2,1}, Y. Chen¹, K. Nishihara¹

M. F. Lubis¹, K. Tanaka³ and S. Kimura^{2,1,4}

¹Department of Physics, Graduate School of Science, Osaka University, Toyonaka 560-0043, Japan

²Graduate School of Frontier Biosciences, Osaka University, Suita, 565-0871, Japan

³UVSOR Synchrotron Facility, Institute for Molecular Science, Okazaki 444-8585, Japan

⁴Department of Materials Molecular Science, Institute for Molecular Science, Okazaki 444-8585, Japan

The Kondo effect leads to exotic physical phenomena due to hybridization between localized *f*-electrons and conductive carriers at low temperatures. Especially, heavy-fermion (HF) systems, in which massive effective carriers appear due to the Kondo effect, have fascinated many researchers [1,2]. Recently, two-dimensional (2D) HF systems have been realized using a molecular beam epitaxy method and it was shown that dimensionality is also important for the character of the HF system [3,4]. However, two-dimensional mono-atomic layer HF material has never been reported. Here, we have studied the electronic structure of a mono-atomic layer HF material, YbCu₂/Cu(111), which is a novel perfect two-dimensional HF system, measured by angle-resolved photoelectron spectroscopy (ARPES).

Clean Cu(111) substrates were prepared by the cycle of Ar⁺ sputtering with an acceleration of 0.5 eV and annealing at a temperature up to 800 K. After checking the sharp peaks and low background of the streak electron diffraction pattern appearing in the reflection high-energy electron diffraction (RHEED), Yb-metal was evaporated with a homemade Knudsen cell. The fabricated YbCu₂ mono-atomic layer has a fractional pattern suggesting a small lattice mismatch of YbCu₂ from the Cu(111) substrate. VUV-ARPES measurement was carried out at BL7U (*hν* = 37 eV) at temperatures of 7 – 130 K.

Figure 1 shows the ARPES intensity plot of YbCu₂/Cu(111) surface along $\bar{\Gamma}-\bar{K}$ of the surface Brillouin zone of YbCu₂/Cu(111). To see the band dispersion above the Fermi level, the ARPES spectra were divided by the Fermi-Dirac distribution function convoluted with the instrumental resolution. A flat band near the Fermi level and several highly dispersive bands are visible. The flat band is attributed to the Yb²⁺ 4*f*_{7/2} final state after the photoexcitation process. The highly dispersive conduction bands are hybridized with the flat Yb 4*f* band near the $\bar{\Gamma}$ point suggesting the appearance of the *c-f* hybridization, which is the spectral evidence of the appearance of HF. Furthermore, angle-integrated photoelectron spectra of YbCu₂/Cu(111) taken at *hν* = 37 eV (*T* = 10 – 130 K) are shown in Fig. 2. The appearing steep peak, pointed by an arrow, is grown and moves to the low energy with decreasing temperature. The peak can be attributed to a Kondo resonance peak usually observed in HF materials [5], therefore, the results suggest the HF formation in

the mono-atomic layer YbCu₂/Cu(111).

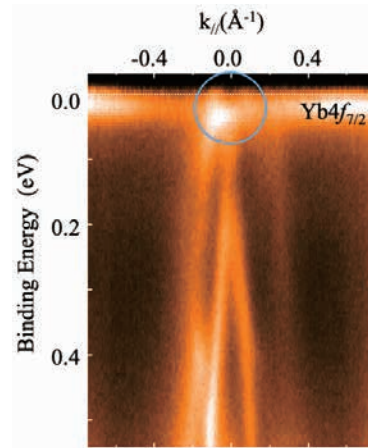


Fig. 1. ARPES band dispersion of YbCu₂/Cu(111) surface along $\bar{\Gamma}-\bar{K}$ taken at *hν* = 37 eV (*T* = 7 K). The photoelectron intensities were normalized by the Fermi-Dirac distribution function convoluted with the instrumental resolution.

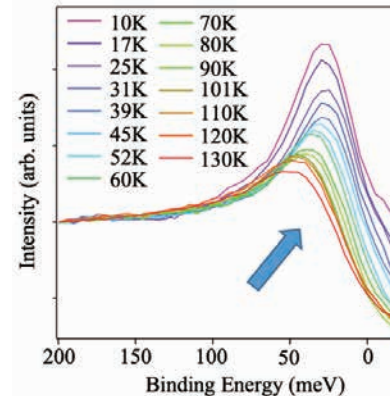


Fig. 2. Angle-integrated photoelectron spectra of YbCu₂/Cu(111) taken at *hν* = 37 eV (*T* = 10–130 K). The arrow indicates the Kondo resonance peak.

- [1] A. C. Hewson, *The Kondo Problem to Heavy Fermions* (Cambridge Univ. Press, Cambridge, 1993).
- [2] P. Coleman, *et al.*, *J. Phys.: Condens. Matter* **13** (2001) R723.
- [3] L. Fernandez *et al.*, *Nanoscale* **12** (2020) 22258.
- [4] M. Ormaza *et al.*, *PRB* **88** (2013) 125405.
- [5] S. Chatterjee *et al.*, *Nat. Commun.* **8** (2017) 852.

BL6U

Region and Element-specific Surface Observation of CVD Graphene on Ir(111)/ α -Al₂O₃(0001) by Photoelectron Momentum Microscopy

E. Hashimoto¹, Y. Onuma¹, F. Matsui² and S. Koh¹¹Aoyama Gakuin University, 5-10-1, Fuchinobe, Chuo-ku, Sagami-hara, 252-5258, Japan²UVSOR Synchrotron Facility, Institute for Molecular Science, Okazaki, 444-8585, Japan

A photoelectron momentum microscopy (PMM) is a complementary characterization tool to conventional methods, e.g. Raman spectroscopy and atomic force microscopy (AFM), for comprehensive and element-specific characterization of 2D materials owing to its multifunctionality. We have demonstrated by valence-band photoelectron spectroscopy (VB-PES) using PMM that graphene grown by low-pressure chemical vapor deposition (LP-CVD) on Ir(111)/ α -Al₂O₃(0001) had high single-crystallinity for several 100 μm^2 [1]. In this study, we performed region and-specific surface observation for graphene by photoemission electron microscopy (PEEM).

Graphene was grown on Ir(111)/ α -Al₂O₃(0001) substrates by LP-CVD using H₂ and CH₄ gases. Fig. 1(a) shows an AFM image (1.0 μm^2) of the graphene surface on Ir(111). Continuous step terraces of the Ir(111), which were the nucleation sites of graphene, were observed. The average step height corresponded to the one-atomic step height of the Ir(111) surface. Wrinkles, which were formed due to the mismatch of the thermal expansion coefficients between graphene and Ir(111), were formed across the step terraces, indicating that graphene domains coalesced and continuous graphene films were formed.

Real space images for graphene/Ir(111) were obtained by PEEM at the linearly polarized soft X-ray beamline BL6U of the UVSOR-III synchrotron [2]. The electronic structure for graphene/Ir(111) were determined by VB-PES. The PEEM images of graphene/Ir(111), which have non-uniformity, are shown in Figs. 1(b) and 1(c). In Fig. 1(b), the photon energy was 85 eV and photoelectron corresponding to the binding energy from 2.0 to 3.5 eV was integrated. Intensity of graphene *M* points contributes the most. Thus, the bright areas in Fig. 1(b) correspond to the areas where graphene exists. The iso-energy cross section of the 2D band dispersion for the bright area in Fig.1(b) by VB-PES is shown in Fig. 1(d). The 6-fold symmetry pattern is attributed to the π band dispersion of graphene connecting the *M* points. Fig. 1(c) shows the PEEM image at the same observation area as Fig.1(b). The photon energy was set to 100 eV. Photoelectron corresponding to the binding energy from 0 to 0.2 eV was integrated. The density of states at the Fermi level of Ir dominates in this condition. Therefore, the bright areas correspond to the area where the Ir surface was exposed. The iso-energy cross section of the 2D band dispersion for the bright areas in Fig.1(c) is shown in Fig.1(e). The pattern with 6-fold symmetry, which corresponds to the energy dispersion of Ir(111),

was observed. The pattern of graphene was not observed, which confirmed that the Ir surface was exposed. We identified areas where covered by graphene and where Ir(111) is exposed, by region and element-specific PEEM for Gr/Ir(111) samples with low single-crystallinity.

In this study, we observed surface irregularities of Gr/Ir(111) samples that were not captured by conventional measurement methods such as Raman spectroscopy and AFM observation, by performing region and element-specific PEEM using PMM. Element-specific measurements using PMM on practical samples are very promising, and the characterization of detailed properties for high-quality Gr/Ir(111) samples is expected.

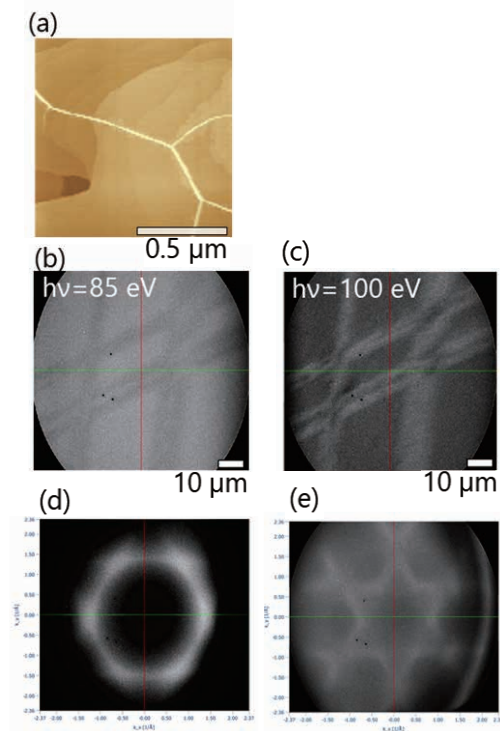


Fig. 1. (a) AFM image and (b)-(c) PEEM images of graphene/Ir(111). Iso-energy cross sections of 2D band dispersion of graphene/Ir(111), with photon energy of (d) 85 eV and (e) 100 eV.

[1] E. Hashimoto *et al.*, Jpn. J. Appl. Phys. **61** (2022) SD1015.

[2] F. Matsui *et al.*, Jpn. J. Appl. Phys. **59** (2020) 067001.

High-resolution angle-resolved Photoemission Study on MnBi₂Te₄/MnBi₂Te₄/Bi₂Te₃ Heterostructure

K. Ishihara¹, H. Nishimichi¹, K. Ide¹, S. Ichinokura¹, K. Tanaka² and T. Hirahara¹

¹Department of Physics, Tokyo Institute of Technology, Tokyo 152-8551, Japan

²UVSOR Facility, Institute for Molecular Science, Okazaki 444-8585, Japan

Topological insulators (TI) are extensively studied recently due to its peculiar properties [1]. The Dirac-cone surface states of TI are protected by time-reversal symmetry (TRS) and backscattering among these surface states is prohibited. But when TRS is broken by application of a magnetic field or incorporating magnetic materials, a gap opening in the Dirac cone is expected and an intriguing phase called the quantum anomalous Hall state can be realized [2]. This phase is expected to show even more exotic phenomena such as the topological magnetoelectric effect. To realize such state, two types of sample fabrication techniques have been employed up to now: (1) magnetic doping while growing the single crystal or thin film of TI [3], and (2) magnetic impurity deposition on the surface of TI [4]. While method (1) was successful and showed evidence of the TRS violation, no one has succeeded using method (2), which should be a more direct way to examine the interaction between the topological surface states and magnetism. We have previously found another novel technique to induce magnetism into TI, namely the magnetic extension effect [5]. By depositing Mn and Se on Bi₂Se₃, we found that Mn and Se are incorporated in the topmost Bi₂Se₃ layer and a novel heterostructure MnBi₂Se₄/Bi₂Se₃ is formed [5]. This heterostructure showed a clear Dirac cone gap of 85 meV and the gap persisted up to room temperature. From magnetic measurements it was revealed that ferromagnetism also persists up to room temperature in this system. Taking all these facts into account, it can be said that this system is promising to observe the quantum anomalous Hall effect at room temperature. However, the Dirac cone gap is not at the Fermi level and there is no systematic method to control the Fermi level position in Bi₂Se₃. Thus, we employed Bi₂Te₃ as the parent TI and have deposited Mn and Te on Bi₂Te₃ to see if magnetic extension can also occur for this system. However, it was revealed that the Dirac cone gap is absent in this MnBi₂Te₄/Bi₂Te₃ system [6], in contrast to the theoretical prediction [7].

Therefore, in the present study, we have measured the band structure of the MnBi₂Te₄/MnBi₂Te₄/Bi₂Te₃ system to verify whether an addition of another MnBi₂Te₄ layer would influence the magnetic property

as well as the Dirac Cone gap opening. The experiments were performed at BL 7U of UVSOR with the photon energy of 19 eV. Figure 1 shows the measured band dispersion at different temperatures.

We found that in addition to the Dirac cone gap opening which was observed from 6.6 K up to room temperature, the lower Dirac cone showed some splitting at 6.6 K. Furthermore, this splitting disappeared once at 160 K, but revived at 250 K. Since the state at higher binding energy showed photon energy dependence, it can be regarded as a bulk state, although our preliminary *ab initio* calculation suggested that it can also be a surface state. This puzzling behavior is unexpected from theory and calls for a comprehensive study on the atomic structure as well as magnetism of the system, which we hope to clarify in the future.

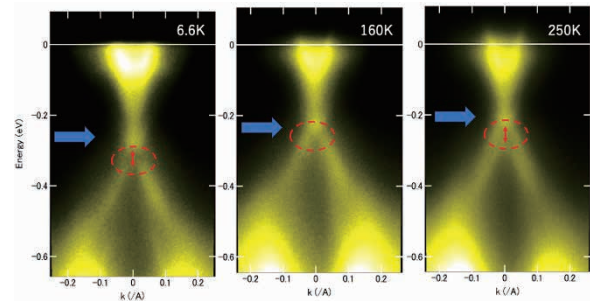


Fig. 1. Band dispersion image of the MnBi₂Te₄/MnBi₂Te₄/Bi₂Te₃/MnBi₂Se₄ hetero structure measured at 6.6 K, 160 K, and 250 K, respectively.

- [1] M. Hasan and C. Kane, Rev. Mod. Phys. **82** (2010) 3045.
- [2] X.-L. Qi and S.-C. Zhang, Rev. Mod. Phys. **83** (2011) 1057.
- [3] For example, C. Z. Chang *et al.*, Science **340** (2013) 167.
- [4] For example, M. Ye *et al.*, Phys. Rev. B **85** (2012) 205317.
- [5] T. Hirahara *et al.*, Nano Lett. **17** (2017) 3493.
- [6] T. Fukasawa *et al.*, Phys. Rev. B **103** (2021) 205405.
- [7] M. Otrokov *et al.*, Phys. Rev. Lett. **122** (2019) 107202; 2D Mater. **4** (2017) 025082.

BL7B

Electrochemical Attenuated Total Reflectance Ultraviolet (EC-ATR-UV) Spectroscopy Applied for Organic Semiconductor / Ionic Liquids Interface

I. Tanabe, Y. Hanamori and K. Fukui

Department of Materials Engineering Science, Graduate School of Engineering Science, Osaka University, 1-3, Machikaneyama, Toyonaka, Osaka 560-8531, Japan

Electric double-layer organic field-effect transistors (EDL-OFETs) have attracted much attention due to their significantly low operating voltage (<1 V) compared to conventional SiO₂-gated OFETs (>10 V). In EDL-OFETs, a high electric field is generated in the EDL that accumulates in the interfacial region between the organic semiconductor and electrolyte, resulting in a low operation voltage. Therefore, the organic semiconductor/electrolyte interface is of particular importance. Recently, we developed a new spectroscopic system, namely electrochemical-attenuated total reflectance (EC-ATR) ultraviolet-visible spectroscopy, which can access the interfacial area [1, 2].

In this study, we fabricated ionic liquid gated organic field-effect transistors (IL-gated OFETs) on the ATR prism. A two-layer single crystalline film of C9-DNBDT-NW was used as an organic semiconductor, and two kinds of ionic liquids (EMIM-TFSI and HMIM-TFSI) were cast on the film. The only difference between EMIM-TFSI and HMIM-TFSI is the length of the carbon chain: two for EMIM and six for HMIM. Au films were evaporated to a thickness as the source and drain electrodes (working electrodes) on both sides of the ATR prism, and a Pt coil and a Pt wire were placed in the ionic liquids as pseudo counter and reference (gate) electrodes, respectively. In our previous study [2], we found that in response to the applied gate voltage, the spectral peaks of the organic semiconductor shifted and bleached, which was correlated with the drain current.

The IL-gated OFETs fabricated on the ATR prism were placed in the sample chamber in BL7B at UVSOR. Figure 1 shows the difference spectra of C9-DNBDT-NW films with EMIM-TFSI or HMIM-TFSI as a function of the applied voltage. Despite the very slight difference in the carbon chain length between EMIM-TFSI and HMIM-TFSI, their spectral behaviors were significantly different.

In the case of HMIM-TFSI (Fig. 1b), spectral bleachings at ~300, 220, 210, 190, and 170 nm were observed. According to TD-DFT calculations, these absorbances are mainly due to electronic excitations in the C9-DNBDT-NW molecule for ~300 nm and in HMIM-TFSI for ~220, 210, 190, and 170 nm. There is a positive relationship between the amount of spectral changes and applied voltage. On the other hand, in the case of EMIM-TFSI (Fig. 1a), no obvious spectral changes were detected. These results indicate a difference in the interaction between the organic

semiconductor and ionic liquid species under electrochemical environments.

The development of the EC-ATR spectroscopic system has the potential to greatly impact the field of electrochemical devices by enabling researchers to access and study the interfacial area between films and ILs, leading to improved understanding of device performance and the development of new, high-performance materials.

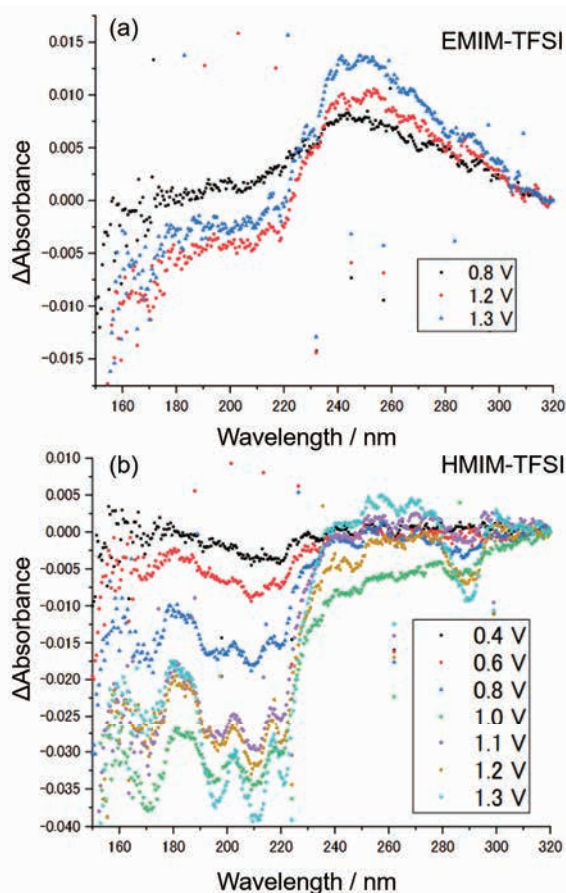


Fig. 1. Difference spectra of C9-DNBDT-NW films with (a) EMIM-TFSI and (b) HMIM-TFSI as a function of the applied voltage.

[1] I. Tanabe, A. Suyama, T. Sato and K. Fukui, *Anal. Chem.* **91** (2019) 3436.

[2] I. Tanabe, I. Imoto, D. Okaue, M. Imai, S. Kumagai, T. Makita, M. Mitani, T. Okamoto, J. Takeya and K. Fukui, *Commun. Chem.* **4** (2021) 88.

UVSOR User 7

